A Stochastic Hybrid Blade Tip Timing Approach for the Identification and Classification of Turbomachine Blade Damage

R.G. Du Toit[a,*], D.H. Diamond[a], P.S. Heyns[a]

[a] *Centre for Asset Integrity Management, Department of Mechanical and Aeronautical Engineering, University of Pretoria, Pretoria 0002, South Africa*

Abstract

Blade Tip Timing (BTT) has been in existence for many decades as an attractive vibration based condition monitoring technique for turbomachine blades. The technique is non-intrusive and online monitoring is possible. For these reasons, BTT may be regarded as a feasible technique to track the condition of turbomachine blades, thus preventing unexpected and catastrophic failures. The processing of BTT data to find the associated vibration characteristics is however non-trivial. In addition, these vibration characteristics are difficult to validate, therefore resulting in great uncertainty of the reliability of BTT techniques. This article therefore proposes a hybrid approach comprising a stochastic Finite Element Model (FEM) based modal analysis and Bayesian Linear Regression (BLR) based BTT technique. The use of this stochastic hybrid approach is demonstrated for the identification and classification of turbomachine blade damage. For the purposes of this demonstration, discrete damage is incrementally introduced to a simplified test blade of an experimental rotor setup. The damage identification and classification processes are further used to determine whether a damage threshold has been reached, therefore providing sufficient evidence to schedule a turbomachine outage. It is shown that the proposed stochastic hybrid approach may offer many short- and long-term benefits for practical implementation.

Keywords: Bayesian Linear Regression, Blade Tip Timing, Damage Classification, Damage Identification, Finite Element Analysis, Hybrid Approach, Stochastic, Turbomachines

1. Introduction

Industry is increasingly confronted by ageing turbines prone to unexpected and catastrophic failure. This raises questions with respect to safety and optimal outage planning [1] and increases the need for enhanced Remaining Useful Life (RUL) estimation [2, 3]. Turbomachine blades, generally low pressure steam turbine blades [4], undergo multiple and severe excitations during normal operation. This commonly leads to reduced fatigue life, the risk of crack formation and ultimately an increased risk of failure. The most dangerous excitation frequencies should ideally be avoided during operation. However, this is not always possible as the turbine rotational speed is ramped up through blade resonant frequencies [5]. Conventional turbomachine blade monitoring techniques include metallurgical assessments or the application of strain gauges. These approaches are nevertheless far from ideal as they are largely intrusive and result in undesirable downtime [6].

*Corresponding author.
Email address: dutor06@gmail.com (R.G. Du Toit)

Blade Tip Timing (BTT) is presently considered the most promising technique for blade monitoring, mainly due to its non-intrusive nature and potential for online application [5]. Furthermore, the use of BTT makes it possible to measure the vibrational state of each blade on a particular row of a rotating disk. This is achieved by using a set of proximity probes placed circumferentially around the casing which sense when a blade passes. The direct application of BTT for vibration monitoring has existed since the 1970s. Yet, this technology is still maturing [5, 7]. Despite being considered promising, scepticism surrounding this method persists. The authors of [8] speculate that unless a BTT technique is made simple and reliable to implement, power plants will not find it attractive to invest in upgrading for safe operation of turbomachines. The following requirements are therefore a prerequisite for BTT techniques to appeal to industry:

1. Simple implementation of testing equipment and post-processing methodologies.
2. Proven reliability in terms of accuracy, robustness and generality of BTT algorithm.

The purpose of this research is to advance the state of the art in BTT technology into a stochastic hybrid approach. The proposed approach uses the outputs of a recently developed BTT technique based on Bayesian Linear Regression (BLR), introduced in [9], and a stochastic FEM based modal analysis. In this approach the FEM based modal analysis supplements the BTT results and the stochastic nature of this approach quantifies the uncertainty of the blade condition. This stands in stark contrast to the vast majority of current BTT research where purely data-driven approaches are used, most of them being deterministic in nature. It should be emphasised that the novelty of the research paper lies in the implementation of the proposed stochastic hybrid BTT approach used for the identification and classification of turbomachine blade damage. The detailed overview of the particular BTT algorithm based on BLR, or BTT for that matter, is therefore not provided. This paper rather intends to highlight the many advantages of adopting a hybrid stochastic BTT approach in an attempt to overcome foreseeable uncertainty in using a purely BTT driven approach for turbomachine blade condition monitoring. In doing so, the many long- and short-term benefits of adopting this hybrid approach as a condition based monitoring technique are discussed.

2. Proposed methodology

Diamond et al. [9] highlight that there is no consensus in published literature as to which BTT data processing method attains the greatest reliability. The reason is partly due to the difficulty associated with turbomachine blade vibration measurements and more so the validation of these measurements. The research of [9] compares three different BTT algorithms on simulated blade vibration data for a number of different cases. This allows the accuracy of each algorithm to be determined under different circumstances. However, the accuracy of practical BTT results may be difficult to determine without prior knowledge of the blade behaviour under different operating conditions. A hybrid approach consisting of a BTT analysis and a stochastic Finite Element Analysis (FEA) is therefore proposed here. Figure 1 outlines the proposed hybrid approach. The application of this hybrid approach aims to alleviate the disadvantages of an individual analysis type while conserving its advantages [2]. The following remarks highlight the advantages of the proposed hybrid methodology:

1. The FEA establishes a baseline for comparison before any BTT tests are performed.
2. The FEA makes it possible to project expected blade conditions, which may not be available from the BTT measurements for quite some time. The use of a FEA therefore enables a predetermined turbomachine blade damage threshold to be established, based on an *acceptable* severity of damage.
3. The BTT analysis accounts for real blade behaviour and aspects not considered using the FEA.

4. Combining the individual approaches may ultimately result in a higher prediction accuracy with regards to the turbomachine blade condition.

Figure 1 indicates that the results from the hybrid approach will be used for two analyses, namely:

1. *Damage identification:* The relative change in the natural frequency of the blade is tracked in order to identify and infer the degree of blade damage.
2. *Damage classification:* The natural frequency and amplitude derived from the BTT results are clustered using predetermined mean values as initial cluster centres. The clustering of these values enable the severity of the blade damage to be classified.

Figure 1 indicates that a blade damage threshold will be established for the aforementioned damage identification and classification analyses. If this threshold is met the operation of the turbomachine should be stopped and relevant maintenance operations should commence. Furthermore, the BTT analysis will be repeated continuously until this threshold is reached. Importantly, the measured BTT data is archived to form a database of the individual blade conditions. The archived data is important in the sense that it establishes a reference condition for the damage identification and classification of the BTT data. The proposed methodology shown in Figure 1 was tested on a laboratory setup and is discussed in detail in the remainder of the article.

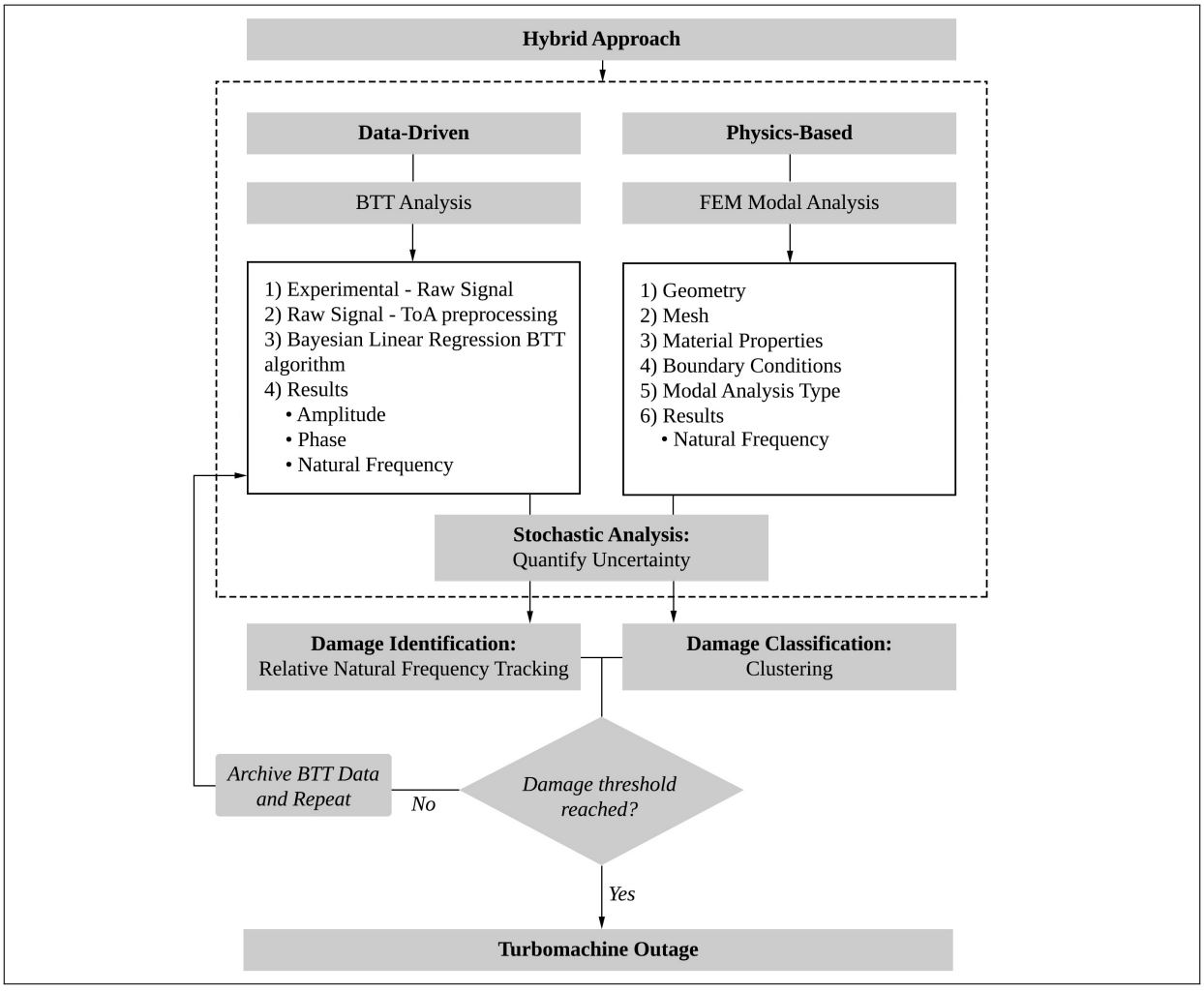

Figure 1: Overview of the proposed hybrid methodology.

3. BTT analysis

3.1. Background and basic principles

The fundamental principles behind BTT are relatively straightforward; the measured Time-of-Arrival (ToA) information of the blades passing a proximity probe is analysed to indicate the vibrational state of each blade. The ToA of a non-vibrating blade is completely dependent on the angular velocity of the shaft. However, a vibrating blade arrives either earlier or later than expected at the proximity probe. This physically translates into the vibrating blade leading or lagging at the proximity probe. The blade tip displacement may be calculated from the change in Angle of Arrival (ΔAoA) of a vibrating blade which is derived by using a Once Per Revolution (OPR) pulse as a shaft reference position [9].

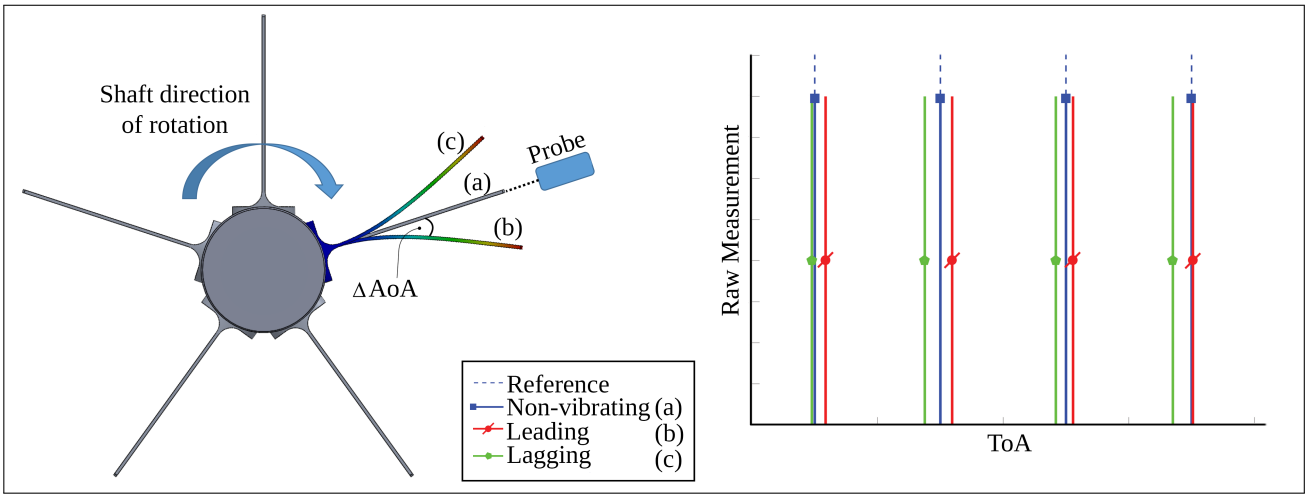

Figure 2: Basic BTT principles.

Figure 2 illustrates the basic BTT principles in terms of what is physically measured using the proximity probe (left) and how these measurements are represented as a ToA (right). BTT may therefore be considered as a three-step process [5]:

1. Acquiring the ToA of the individual blades at each proximity probe.
2. Deriving the blade tip displacements from the ΔAoA.
3. Analysing this data and extracting the desired results.

3.2. BTT algorithm

Extracting the blade vibration from ΔAoA is a non-trivial task. This is due to the measured signals being aliased or sub-sampled, therefore inhibiting conventional signal processing. Many BTT algorithms have been developed to overcome these difficulties and are divided into two main categories [5, 9]:

1. *Indirect methods:* The maximum amplitude and corresponding frequency at resonance is determined during transient operating conditions. Only one or two proximity probes are required.
2. *Direct methods:* The maximum amplitude at each measured rotational speed is determined during steady state operating conditions. At least four proximity probes are normally used.

This article considers a recently developed direct BTT method based on statistical infererence. This technique employs BLR and is attractive for use in practical applications for a number of reasons [9]. Firstly, the amplitude and phase may be determined at each measured rotational speed.

This results in a detailed picture of these parameters and their changes over the operating domain. Secondly, the processed data considers the whole range of inferential solutions, therefore resulting in a stochastic solution. Lastly, the stochastic nature of the processed data allows one to establish confidence intervals for the amplitude and phase. This allows noise tolerant behaviour for this technique.

3.3. Experimental investigation

The experimental investigation generated practical data for the use in the hybrid approach. More so, the experimental investigation tested the ability of the BLR based BTT technique to provide the relevant information for the blade damage identification and classification outcomes. In order to do so, incremental blade damage was introduced to selected blades and synchronous blade vibrations were induced in the experimental investigation. Synchronous blade vibrations occur as an Engine Order (EO) of the shaft rotational speed and is generally a result of the fluid-flow path being obstructed by a multiplicity of structural components [10]. This category of blade vibration is notoriously difficult to measure, mainly due to the similar tip displacements being measured for each revolution, therefore resulting in the redundancy of multi-revolution measurements. The details of the experimental investigation follows.

Experimental setup

The experimental setup broadly consisted of the following: rotor assembly, excitation mechanism, sensors, an acquisition system and a signal generation system. *LabVIEW* 2015, with associated *National Instruments* voltage output card, were used to generate signals controlling the motor speed. For a sanity check, the sensitivity of the chosen BTT technique to sampling frequency was investigated by using two independent Data Acquisition Devices (DAQs). The *OROS OR35* DAQ with *NVGate* software had a sampling frequency limitation 65.536 kHz for the required number of input channels. The *HBM Genesis High Speed DAQ*, with *Perception* software, had a much higher sampling frequency at 1 MHz as well as a higher resolution. Figure 3 highlights the main components of the experimental setup.

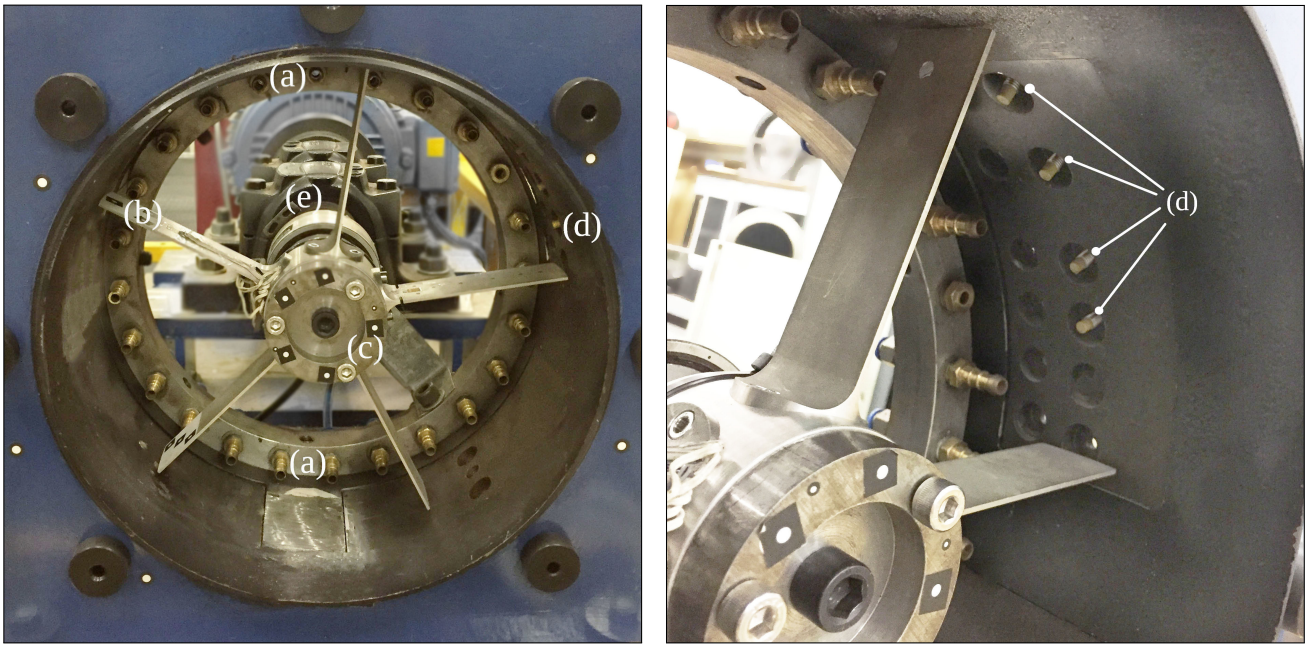

(a) Rotor assembly.

(b) Casing with proximity probes.

Figure 3: Experimental setup.

The components of the experimental setup, with reference to the labels in Figure 3, are as follows:

a. Compressed air supply nozzles for blade excitation (top and bottom of casing).

b. Bladed assembly comprising 5 aluminium 6082 T6 simplified blades. The blades have a root-to-tip length of 132mm, a width of 40mm and are 2mm thick (as indicated in Figure 4).

c. Central blade hub with slip ring mounting holes (for strain gauge wiring). The strain gauges were used for the initial sanity check of the BTT results of the damaged blade.

d. Rotor casing with 4 irregularly spaced eddy current probes. The irregular spacing of these eddy current probes was informed by the recommendations made in [9].

e. Shaft connected to a motor with variable speed control.

Experimental methodology

Figure 1 highlights that the results from the chosen BTT technique are used to identify and classify blade damage. In order to do so, the BTT technique based on BLR was first tested in terms of detecting a noticeable change in the natural frequency of a blade. Discrete damage was introduced to a single blade as part of a preliminary test. Distinct differences were noticed between the healthy blades and the damaged blade with regards to the resultant amplitude, phase characteristics and derived natural frequency. The details of the post-processing procedure used to derive these vibrational characteristics are presented in Section 3.4. As expected, the natural frequency proved to decrease as the increased damage reduced the blade stiffness. Subsequent to this, a more controlled experimental procedure was followed to test the proposed hybrid approach with regards to identifying and classifying blade damage. The following experimental procedure was followed for the BTT analysis of the hybrid approach:

1. The rotor assembly blades were numbered to keep a record of the blade specific results. Figure 5a gives an example of the measured voltage pulses at the four proximity probes. Figure 5a also shows the extracted ToAs at a chosen trigger level, as a result of linear interpolation. The raw proximity probe signals indicate that a specific blade was slightly longer than the others. This blade was used as a reference blade and referred to as *blade 1*. Blade 2 was selected as the test-blade.

2. An initial modal analysis was performed using a FEA to determine where the maximum stress concentration occurs for the first bending mode (only the first bending mode was considered for this investigation). Figure 4a shows that the maximum stress concentration for the first bending mode occurs directly and slightly above the blade fillet. The discrete damage was therefore introduced in this region, due to crack formation as a consequence of fatigue commonly occurring in maximum stress concentration regions [11, Chapter 6].

3. The size of the incremental damage introduced to blade 2 corresponded to the values shown in Table 1. The relative crack sizes were computed as a percentage of the total width (40mm) of the blade. The small size of the discrete damage aimed to test the ability of the BTT technique to track small changes in the natural frequency of the blade due to the introduced damage.

4. The shaft speed was ramped up from 1195 RPM to 1330 RPM and down again in order to pass through the blade resonant frequencies. The resonant frequencies across the motor operational speed range were predetermined from a Campbell diagram generated by a simple FEM modal analysis. This FEM modal analysis does not form part of the proposed hybrid approach outlined in Figure 1. The strain gauges shown in Figure 4b were also used as an initial sanity check of the blade natural frequencies which were extracted using a Fast Fourier Transform (FFT) of the recorded time-voltage signal. The compressed air supply (begind the top and bottom of the rotor) excited the first mode of vibration of the blades during rotation.

5. The experimental BTT tests were repeated 6 times for each of the damage increments shown in Table 1 (72 tests in total). The repetitive nature of the experiments aimed to determine the robustness of the chosen BTT technique. In order to control the comparison of the extracted blade phase results between tests, it was important to synchronise all the measured proximity probe signals with respect to a certain shaft encoder pulse. This synchronisation enabled all the proximity probe signals for all the tests to start on the same pulse. Figure 5b shows that blade 1 at probe 1 was used for this synchronisation. The sensitivity of the BTT measurement accuracy to data acquisition sampling frequency was investigated by performing 3 tests per DAQ for the particular damage increment.

6. The ToAs were extracted from the raw voltage shaft encoder and proximity probe signals at a chosen trigger level. Figure 5a gives an example of the extracted proximity probe signal ToAs for the various blades. The extracted ToAs were then used directly in the BTT post-processing to derive the amplitude, phase and associated blade natural frequencies (discussed in Section 3.4).

In summary a few important aspects with regards to the experiment are highlighted as follows. Discrete damage was introduced incrementally from an originally healthy state, with the most severely damaged blade shown in Figure 4b. The introduction of incremental damage aimed to test the ability of the proposed hybrid approach with regards to the damage identification and classification processes. These processes require the derivation of the blade vibrational characteristics; i.e. amplitude, phase and associated natural frequencies. The derivation of these characteristics follows in Section 3.4. The incremental change in the size of the introduced damage was kept small. This aimed to test the ability of the proposed BTT approach to track small changes in the natural frequency of the blade as the size of the discrete damage was increased. The strain gauges along with an FFT were merely used as an indicator of what level of damage would result in a desired change in the blade natural frequency, as well as a sanity check of the natural frequencies derived from the BTT data. Furthermore, it should be reiterated that the initial FEM modal analysis does not form part of the proposed hybrid approach. The initial FEM modal analysis essentially highlighted where the maximum stress concentration would be for the first bending mode of vibration as well as the associated natural frequency to choose the relevant shaft speed profile.

The introduced incremental damage lengths are shown in Table 1 below. The damage severity classifications in this table are discussed as part of the damage classification procedure in Section 5.2. Images of the test blade (blade 2) and the raw voltage signals follow in Figures 4 and 5 respectively.

Table 1: Incremental discrete damage introduced to blade 2.

Damage Increment	**Crack Size (mm)**	**Damage Severity Classification**
1	0	Non-severe *(Range of damage I)*
2	0.90	
3	1.11	
4	1.28	
5	1.58	
6	1.81	
7	3.11	Mid-severity *(Range of damage II)*
8	3.87	
9	5.60	
10	6.97	Severe *(Range of damage III)*
11	8.30	
12	8.61	

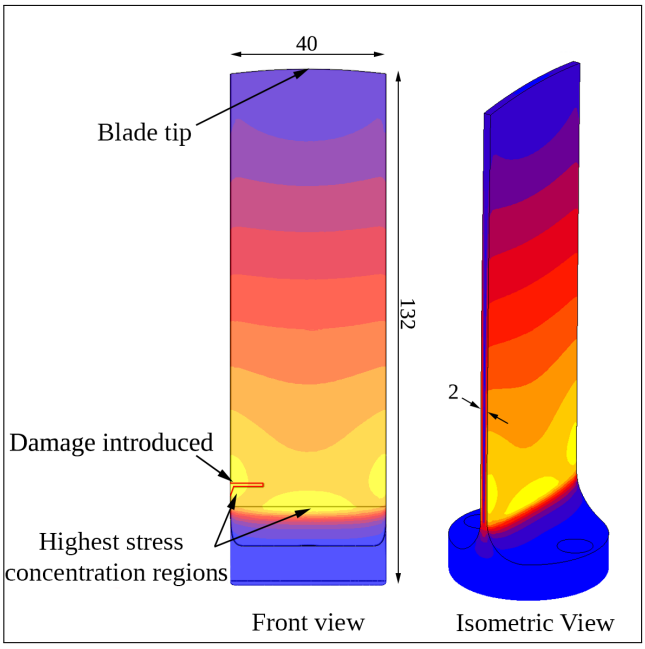

(a) Highest stress concentration region check (mode 1).

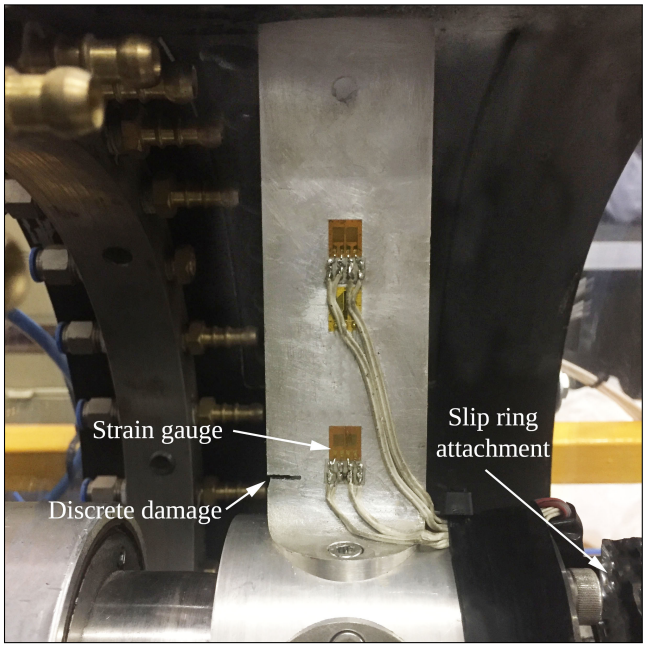

(b) Test blade with maximum incremental damage.

Figure 4: Test blade.

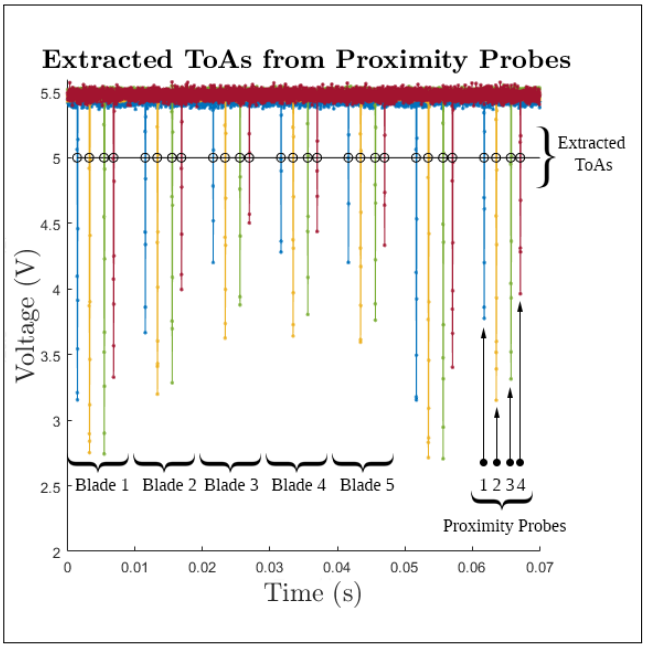

(a) Example of raw proximity probe signals.

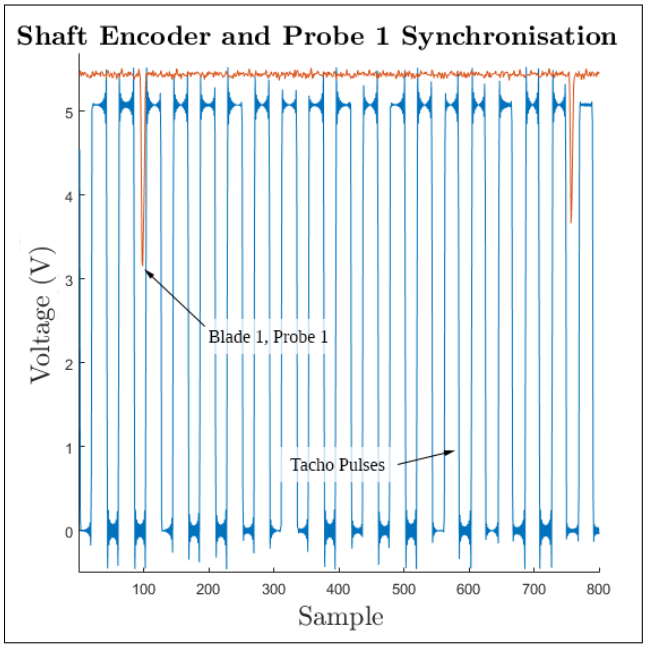

(b) Synchronisation of raw proximity probe pulses.

Figure 5: Measured voltage signals.

3.4. Post-processing

The raw voltage signals for the proximity probes and shaft encoder are converted to ToA values. The shaft encoder ToAs are used to derive the shaft speed. The blade tip displacements are derived from the per revolution ΔAoA values, for each blade and at a specific proximity probe. Figure 6 illustrates the derived blade tip displacement at specific shaft speeds. Peaks in the tip displacement clearly occur at two time instants. These peaks are localised and are used to derive the vibration characteristics of a specific blade. The blade specific proximity probe data is then combined to statistically infer the vibration characteristics using a BLR technique. An illustration of the tip displacements of a single blade at a proximity probe is given in Figure 6.

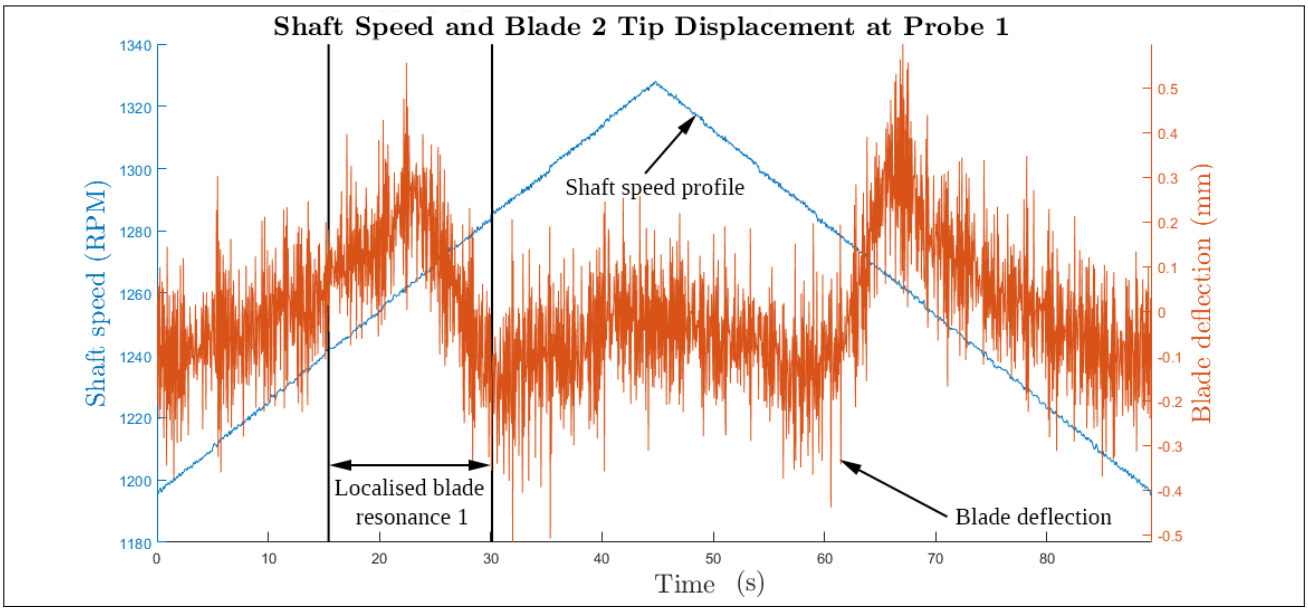

Figure 6: Tip displacement compared to the rotational shaft speed.

The BTT technique based on BLR assumes a Single Degree-of-Freedom (SDoF) model for the blade vibration. Equation 1 shows the formulation of this model for the blade tip displacement (x), at a specific time (t), Engine Order (EO) and angular frequency (ω):

$$x_i(t) = A_i \cdot \cos(\omega \cdot t_i) + B_i \cdot \sin(\omega \cdot t_i) + C_i \tag{1}$$

$$\text{where} \quad \omega = EO \cdot \Omega \tag{2}$$

BLR is specifically used to infer the values of the constants A, B and C as probabilistic quantities. Importantly, the values in Equation 1 are solved for each revolution (indicated by the subscript i) at a corresponding shaft speed (Ω). Equation 2 shows that the correct estimation of the EO is critical in order to infer the *true* vibration characteristics. The BTT method incorporating BLR relies on a probabilistic approach to determine the EOs, whereby a range of EOs are provided to the algorithm. The probability, along with the associated variance, of each supplied EO to fit the blade tip displacement measurements are then computed. The EO with the highest probability is chosen for further use in the BLR processing. Figure 7 shows an example of the solution for Equation 1 (with the standard deviation from the mean solution also shown). This figure corresponds to a short time increment of the localised resonance seen in Figure 6. In Figure 7 the resultant fitted curves for the blade tip displacement have discontinuities. These discontinuities are indicative of the BLR being performed for each revolution. Figure 7 shows that the superimposed tip deflection measurements result in aliasing which is present in the measured BTT data.

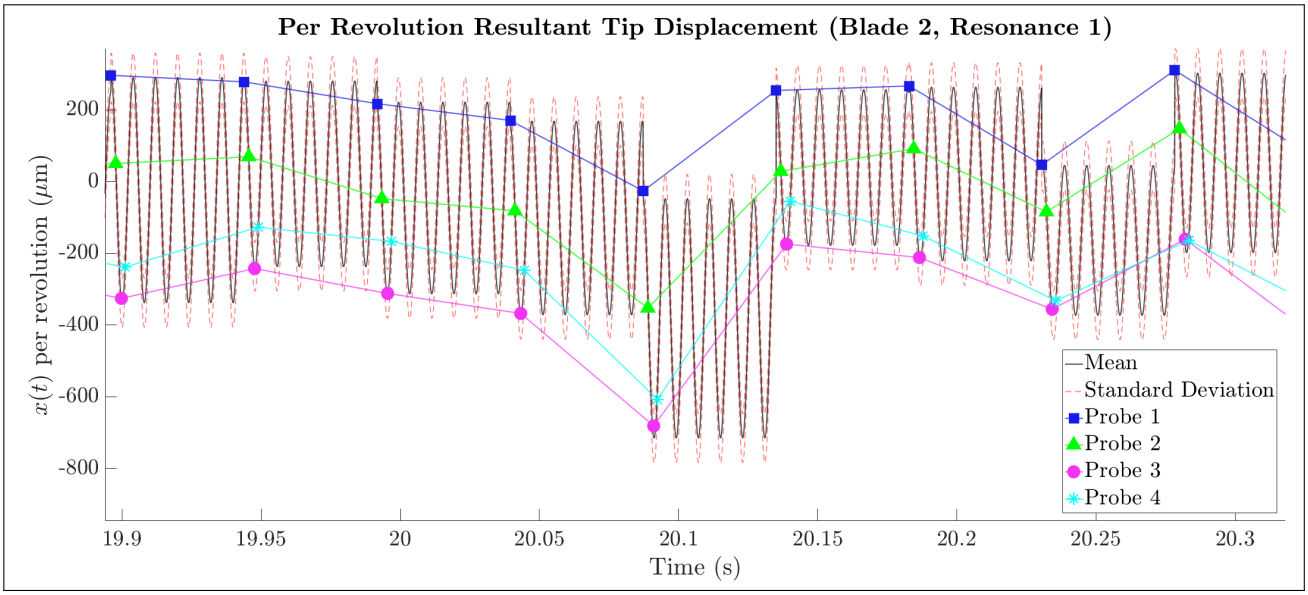

Figure 7: Localised resonant tip displacement.

An advantage of the BLR BTT method is that equidistant probe spacing is not required. In fact, it is mentioned in [9] that BLR for this particular problem works best when the proximity probes are irregularly spaced. Equation 3 again highlights that the inferred SDoF equation parameter set, $\mathbf{x}$, is solved for each revolution, i. This parameter set forms part of a multivariate normal distribution with associated mean, $\boldsymbol{\mu}_i$, and covariance matrix, $\boldsymbol{\Sigma}_i$, as shown by Equation 3. The results of Equation 3 are used to derive the amplitude and phase. The major advantage of using the BLR BTT method is that uncertainty is incorporated in the derivation of the SDoF model parameters. This allows the amplitude and phase values to be determined stochastically rather than deterministically, as required by the hybrid approach outlined in Figure 1.

$$\mathbf{x}_i = \begin{pmatrix} A_i \\ B_i \\ C_i \end{pmatrix} \quad \boldsymbol{\mu}_i = \begin{pmatrix} \mu_{A_i} \\ \mu_{B_i} \\ \mu_{C_i} \end{pmatrix} \quad \boldsymbol{\Sigma}_i = \begin{pmatrix} \Sigma_{AA_i} & \Sigma_{AB_i} & \Sigma_{AC_i} \\ \Sigma_{BA_i} & \Sigma_{BB_i} & \Sigma_{BC_i} \\ \Sigma_{CA_i} & \Sigma_{CB_i} & \Sigma_{CC_i} \end{pmatrix} \tag{3}$$

Figure 8 summarises the procedure used to calculate the resultant stochastic amplitude and phase values. Again, this was done for each shaft revolution of the localised resonance. The amplitude and phase values were calculated using Equations 4 and 5 respectively [12]. Figure 8 also emphasises that the BLR solution set has an associated normal distribution for each of the parameters. Using these normal distributions in a Monte-Carlo Simulation enabled the amplitude and phase results to also have an associated normal distribution. This was done by using 10000 random samples for A and B associated with the respective multivariate normal distribution. These random values were substituded in Equations 4 and 5 to find a range of possible solutions for the amplitude ($\hat{A}$) and phase (ϕ). In essence, the Monte-Carlo analysis is a tool for combining a number of distributions [13], thus enabling the amplitude and phase results to be stochastic rather than deterministic. This allows the uncertainty of these results to be quantified with associated confidence intervals.

$$\hat{A}_i = \sqrt{A_i^2 + B_i^2} \tag{4}$$

$$\phi_i = \arctan\left(\frac{B_i}{A_i}\right) \tag{5}$$

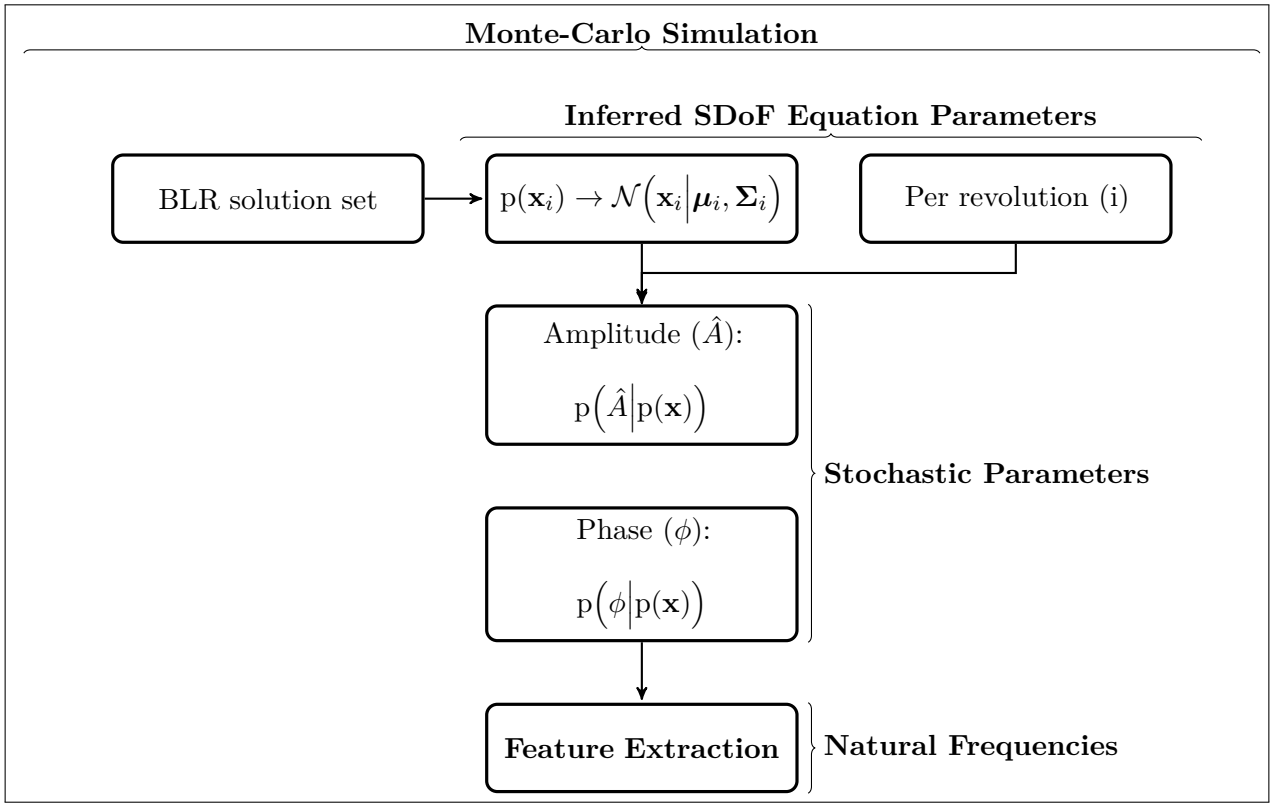

Figure 8: Monte-Carlo Simulation overview.

Referring back to Figure 1, the desired outcomes are to track changes in the blade natural frequencies and classify blade damage by means of clustering. These outcomes will in essence culminate in a decision whether a damage threshold is reached. Figure 8 shows the next step in doing so is to determine the associated natural frequency of the blade by means of *feature extraction*. The mean amplitude and phase values were considered for the feature extraction, however, confidence intervals of these values were also established in order to get a sense of associated uncertainty. The mean values over the localised resonant frequency range were grouped together for the particular blade damage increments previously discussed. The extracted features were as follows:

1. The maximum amplitude and associated frequency as indicated by Equation 6. Henceforth, this frequency is referred to as the natural frequency derived from the amplitude.

$$f_{n_{\hat{A}}} = f(\vartheta) \quad \text{where} \quad \vartheta = \max_{i \in N} \hat{A}_i \tag{6}$$

2. The mid-point of the 180° change in phase angle and associated frequency as indicated by Equation 7. This natural frequency is specifically calculated at the midpoint between the lower frequency (f_l) and upper frequency (f_u) where a 180° change in phase angle is located over the entire localised resonance domain. This is typically characterised by a sudden shift in the phase from -90° to +90° (or $-\frac{\pi}{2}$ to $+\frac{\pi}{2}$ in radians). Henceforth, this frequency is referred to as the natural frequency derived from the phase.

$$f_{n_{\hat{\phi}}} = f(\varrho) \quad \text{where} \quad \varrho = \frac{f_u + f_l}{2} \quad \text{subject to} \quad \Delta\hat{\phi} \geq \pi \tag{7}$$

Furthermore, the feature extraction may be achieved using two approaches. Firstly, the features may be extracted for each of the individual signals of a particular test case. As a result the individual natural frequencies corresponding to the amplitude and phase may be found for each test case. The second approach involves combining the mean amplitude and phase signals for a number of the same tests. The feature extraction is then performed on the combined signals. This approach may be more beneficial in industry where the archiving of BTT results is essential.

Figure 9 highlights the BTT results of a preliminary investigation whereby 30 of the same BTT measurements were taken of the undamaged blade. This investigation aims to demonstrate what may be expected from a single BTT measurement. Figure 9 is a Multivariate Probability Density Function (PDF) of the test blade natural frequencies extracted from the BTT amplitude results. The univariate results of this investigation are summarised in Table 2. The results from Figure 9 and Table 2 indicate that uncertainty exists for the individual measurements. Inevitably, this needs to be accounted for.

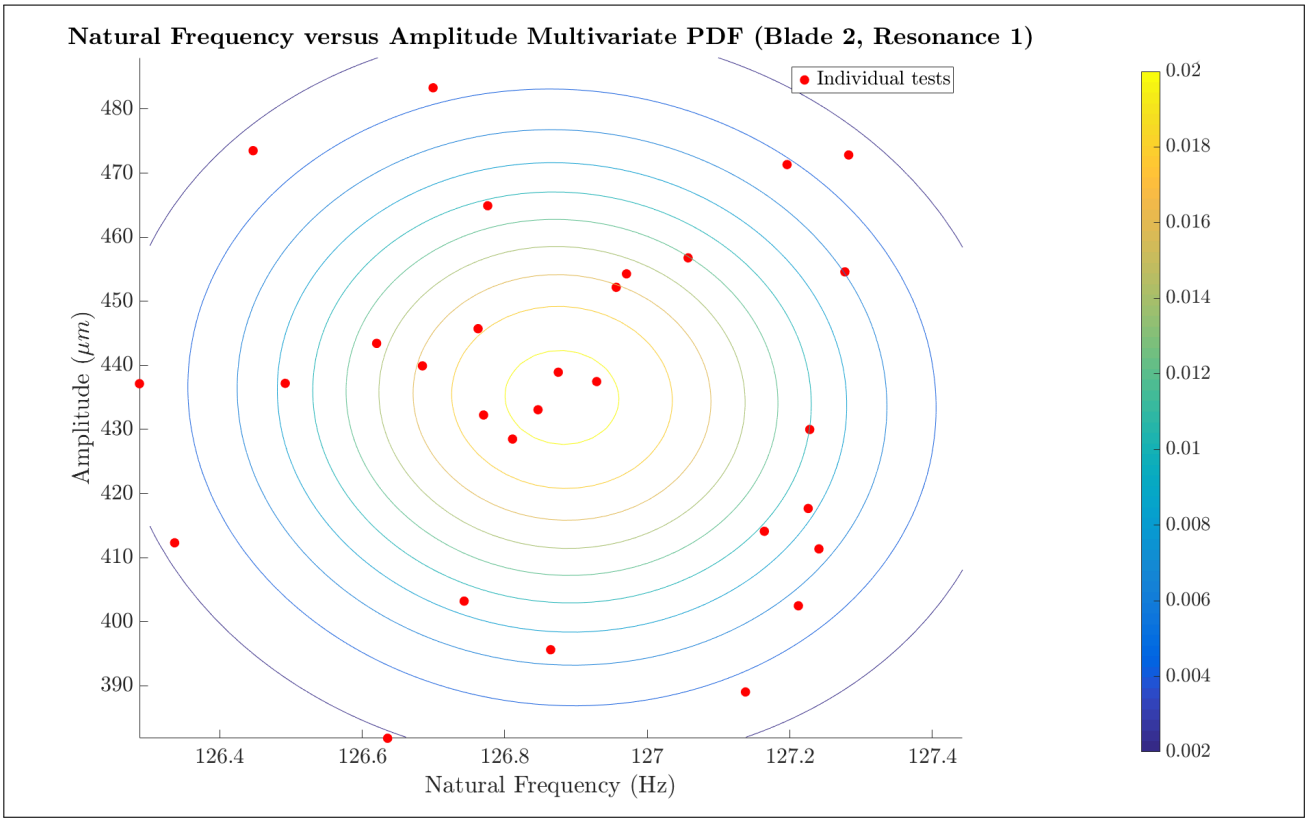

Figure 9: Scatter plot of BTT amplitude and natural frequency results for blade 2 (preliminary investigation).

Table 2: Amplitude and natural frequency results (from a univariate analysis of these parameters).

Value	**Amplitude ($\hat{A}$)**	**Natural Frequency (f_n)**
Mean	435	126.88
Standard Deviation	26.513	0.289

Figure 10 shows the strain gauge FFT results for blade 2 in bending mode 1. The use of strain gauges in this preliminary investigation was merely a sanity check of the extracted natural frequency of the BTT results. The mean natural frequency of the BTT results shown in Table 2 is very close to what is shown for the strain gauge in Figure 10. It is clear that performing a number of the same tests and extracting the features does help to establish a more confident indication of the natural frequencies.

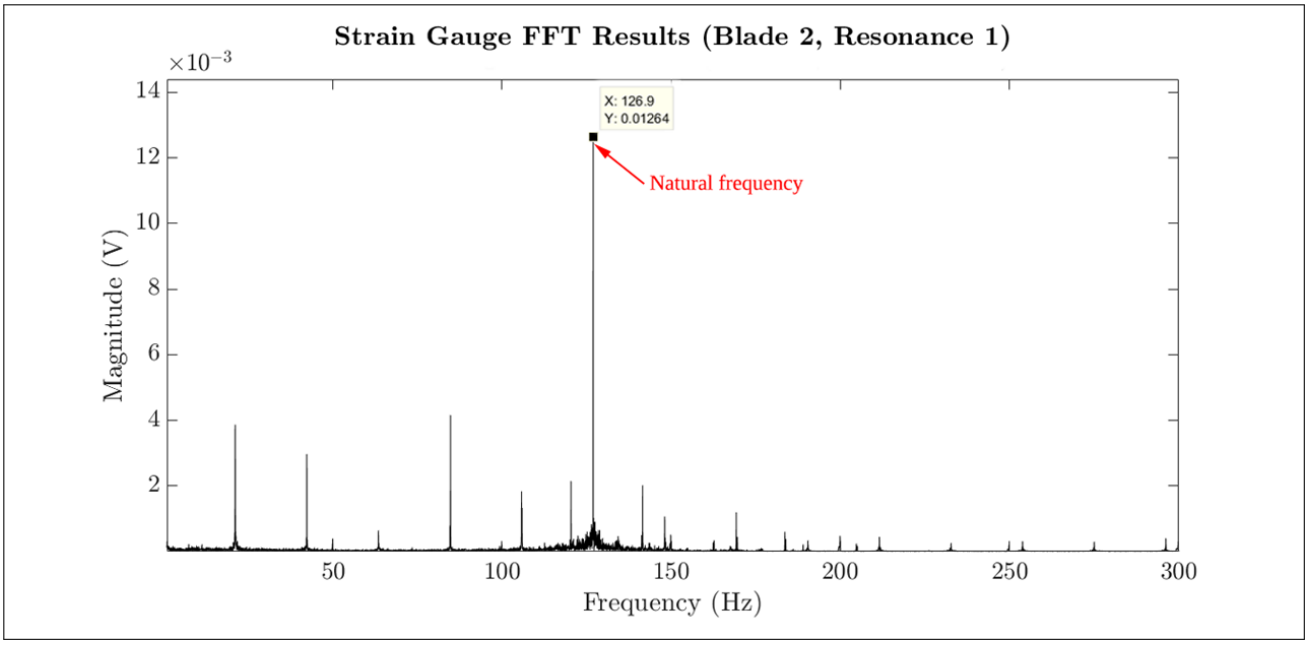

Figure 10: Strain gauge FFT results for blade 2 in bending mode 1 (preliminary investigation).

It is clear that the uncertainty of the BTT measurements needs to be accounted for during the blade damage identification (relative natural frequency tracking) and damage classification (clustering). The proposed hybrid approach aims to account for the uncertainty of the BTT measurements by incorporating a stochastic FEM modal analysis to project expected natural frequencies associated with a certain discrete damage increment. This is discussed in detail in Section 4. Furthermore, the stochastic nature of the BTT and FEM analyses enables confidence intervals to be established around the extracted mean values, thus identifying measurements with greater uncertainty.

4. FEM modal analysis

4.1. Background

A three-dimensional (3D) FEM modal analysis was performed to determine the likely blade resonances at the particular operational speeds. The authors of [14] performed a similar FEA; specifically on a low-pressure turbine bladed disk model to estimate the blade natural frequencies and mode shapes. In this study centrifugal loads were accounted for by applying angular velocities to all the elements. Thermal loads were accounted for by varying the associated material properties. The temperature dependence of the material properties, for Young's modulus and density, is indicated in Equations 8 and 9 respectively. The mathematical relationship for the dependence of the natural frequency on these material properties is shown in Equation 10 [14]. For this particular study, the FEM modal analysis results aim to supplement the BTT results, therefore establishing the basis of a hybrid approach.

$$E \propto \frac{1}{T} \tag{8}$$

$$\rho \propto \frac{1}{T} \tag{9}$$

$$f_n = \mathrm{f}\left(\sqrt{\frac{E}{\rho}}\right) \tag{10}$$

The use of a commercial Blade Vibration Monitoring System (BVMS) on the final stage of the low-pressure steam turbine is outlined in [15]. This report mentions that BTT methods employed by commercial BVMSs offer a viable approach for managing risks associated with turbine blade vibrations. Importantly, it is noted that although the use of BVMS offers a continuous monitoring capability of the blades, many of the effects of the blade vibration risks may only be noticed over long-term monitoring. For this reason it is suggested that the blade modelling that is critical for the interpretation of the BVMS (or BTT) results needs to be performed using FEA.

4.2. Analysis principles

For the current investigation the FEM modal analysis aims to establish a reference of expected natural frequencies, corresponding to the specific operating conditions outlined in the experimental investigation (Section 3.3). The commercial software, *MSC Marc Mentat 2016*, was used to perform the FEA. The *Lanczos* modal solution method was specifically used to compute the desired natural frequencies and amplitudes for the simplified blade model. Figure 1 highlights that a stochastic rather than deterministic FEM modal analysis should be performed to model uncertainty. The discrete damage modelled in the FEA was introduced in 12 incremental stages, which correspond to the damage of the experimental test blade. The discrete crack sizes and locations were, in essence, replicas of what was introduced experimentally (as shown in Table 1). However, slight variations in the angle and size (length, width and height) were introduced to the various increments. This was done to account for small inaccuracies of the true crack measurements. Furthermore, the slight variations aimed to account for uncertainties that would inevitably be present if the exact location of the damage was assumed. The damage was merely introduced at this location as it was shown that this is where a *natural* crack would most likely form (refer to Figure 4a). Blade stiffening was accounted for by applying an angular velocity to the model. The reference material properties corresponded to what was reported by the manufacturers of the blades for *Aluminium 6082 T6* at room temperature. Slight variations in the material properties and centrifugal load were introduced to the model to further account for uncertainty.

4.3. Modelling

This section describes the main components of the FEA modelling, namely: the geometry, mesh, material properties and applied boundary conditions. Figure 11 describes how the five-bladed rotor experimental setup was simplified in the FEM environment.

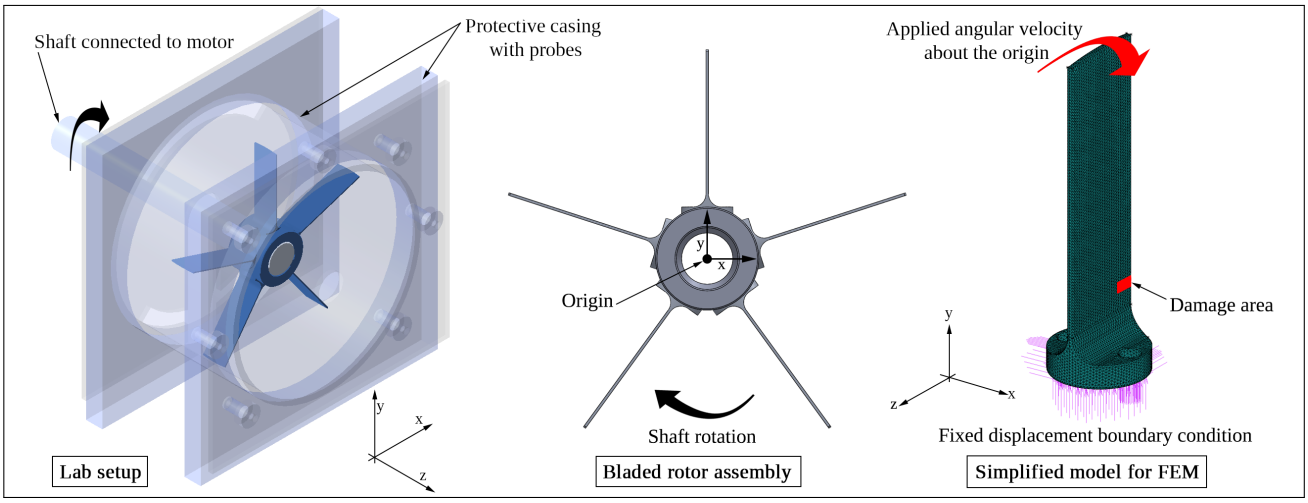

Figure 11: Overview of the simplified FEM model.

Geometry and Mesh

Only a single blade was considered for the solid 3D FEA. The generated mesh consisted of at least 89885 elements for the most basic geometry. Local mesh refinement was applied around the discrete crack for the damaged blades. Ten-noded tetrahedral elements (full-integration, type 127) were used for all the analyses. The discrete crack was introduced in the damage area shown in Figure 11. The first increment corresponds to the healthy blade and the twelfth increment to the most severe damage. As a result, the FEA results were grouped according to the damage increments. The reference discrete cracks were introduced to the blade parallel to the z-axis. For all the damage increment groups, the angle of the applied crack was varied by approximately 10° and the sizes of the cracks around 12% to model uncertainties in measurements. Samples of these parameters were randomly selected from a uniform distribution within this 10° and 12% variation range. For consistency, the same variations were applied for each successive damage increment of the FEA.

Material

The reference material properties at room temperature for Aluminium 6082 T6 are shown in Table 3. The temperature in the laboratory where the experiments were conducted was monitored. It was reported that a more or less consistent ambient temperature (room temperature) was maintained due to the air-conditioning. Uncertainty was, however, incorporated into the FEA by varying the material properties within 12% of the reference values. Again, samples of these parameters were randomly selected from a uniform distribution within the specified variation range. Inevitably, a number of analyses were conducted for each damage increment, therefore resulting in a stochastic rather than deterministic modal analysis.

Table 3: Aluminium 6082 T6 material properties at room temperature.

Temperature $\boldsymbol{T}$ $\boldsymbol{(^{\circ}C)}$	**Density** $\boldsymbol{\rho}$ $\boldsymbol{(\frac{kg}{m^3})}$	**Elastic modulus** $\boldsymbol{E}$ $\boldsymbol{(GPa)}$	**Poisson's ratio** $\boldsymbol{\nu}$
22	2710	71	0.33

Boundary conditions

The applied boundary conditions were representative of the blade attachment to the hub, therefore displacements were constrained at the contact points. Furthermore, the blade stiffening was accounted for by applying a structural centrifugal load to the model. This was done by applying an angular velocity to all the elements. The angular velocities were varied according to the shaft speed range shown in Figure 6 for all the increments. The reference axis for the centrifugal load corresponds to the origin depicted in Figure 11.

4.4. Post-processing

The natural frequency and mode shapes of the first 3 modes were subsequently computed. Figure 12 gives sample contour band plots of these modes for the undamaged and most severely damaged blades using the reference model properties. Modes 1 and 3 clearly correspond to bending mode shapes. Mode 2 corresponds to a torsional mode shape. The changes in natural frequencies between these extremes are approximately 4Hz, 19.9Hz and 9.2Hz for modes 1, 2 and 3 respectively. Interestingly, all the undamaged blades have a fairly symmetrical displacement contour band pattern. However, for the most severely introduced damage, only mode 1 shows contour band patterns which remain fairly symmetrical.

Mode 3 shows a completely different contour band pattern, with the maximum displacement changing from the centre of the blade to the upper-left tip. It is clear that the blade exhibits increased *twist* as the discrete damage is increased on a single side. However, for the purposes of this investigation only mode 1 was considered. This corresponds to what is suggested by [16] in terms of which mode has the greatest contribution to fatigue blade damage.

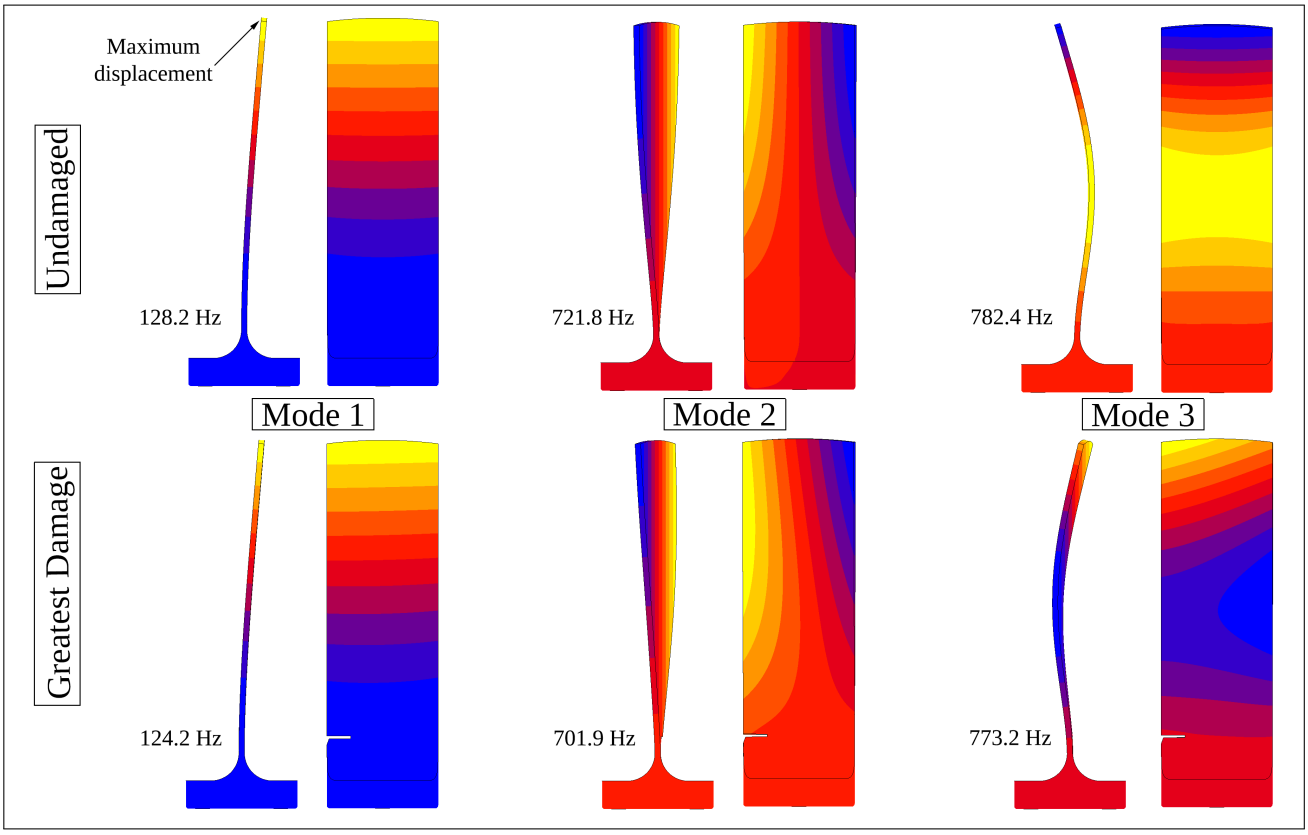

Figure 12: Mode shapes indicating the displacement contour bands.

The FEA was implemented in such a way that it was possible to conduct an investigation similar to what was done experimentally for the BTT testing. Each damage increment in the FEM modal analysis also consisted of six independent tests. For each of these tests, the model parameters (discrete crack geometry, material properties, centrifugal load) were varied according to what was presented in Section 4.3. The variation of these model parameters resulted in a variation of the natural frequencies obtained for each test within a particular damage increment group. This further enabled a mean, with associated confidence intervals around the mean, of the natural frequencies to be found for each damage increment. Advantageously, this process enabled the uncertainties of the various parameters in the FEA model to be quantified, therefore being more representative of what might be expected from the BTT analysis.

5. Results and discussion

This section presents the results obtained for the BTT and FEA methodologies. More importantly, the use of these results in the hybrid approach shown in Figure 1 is discussed. Ultimately, the goal is to determine whether the practical BTT results are indicative of a damage threshold being reached. Figure 1 indicates that damage identification (relative natural frequency tracking) and damage classification (clustering) procedures are employed to determine if this threshold is reached.

The remainder of this section therefore presents and discusses the results from the damage identification (Section 5.1) and damage classification (Section 5.2) procedures. The following points should be noted before these procedures are discussed in detail:

- Incremental discrete cracks were physically introduced to a test blade (blade 2) in the rotor setup. The changes in sizes of these discrete cracks were not constant amongst the various incremental steps. The cracks were measured for each incremental step and these measurements were subsequently replicated in the geometry for the FEM modal analysis.
- Repetitive BTT tests were performed for each damage increment. Half of the measurements used the *OROS DAQ* (65.536 kHz) and the other half used the *Genesis DAQ* (1 MHz) to determine the sensitivity of the BLR BTT technique to the sampling frequency.
- Feature extraction was performed on the processed BTT amplitude and phase results to determine the natural frequencies for the various tests. Only the natural frequencies corresponding to the first bending mode are considered.
- The FEA replicated the experimental tests and modal analyses were performed stochastically by varying a number of parameters. The natural frequencies corresponding to the first bending mode were recorded.

5.1. Damage identification

For this particular application damage identification involves: tracking the relative change in the natural frequency of the blade to identify and infer the degree of discrete blade damage. The change in natural frequency from a reference state (in this case an undamaged state) is quantified. The aim is to determine whether a blade damage threshold has been reached. Figure 1 shows that this decision is made using the outputs of the proposed stochastic hybrid approach and consequently results in a decision of whether a turbomachine outage should be scheduled. The challenge is that the discrete crack sizes of the blades are not known while online BTT measurements are made. It is also impractical to schedule a turbomachine outage and to inspect the individual blades, unless there is sufficient evidence that suggests that a certain blade has reached a critical level of damage; i.e. a *damage threshold*. It is therefore essential to infer the degree of blade damage from the processed BTT results. This section presents the damage identification process by discussing two procedures, namely:

- *Procedure 1* is purely used to demonstrate the relative natural frequency tracking results of the BTT and FEM modal analyses. In doing so, the ability of the proposed hybrid approach to track small changes in the blade natural frequency, due to the changes in the size of the discrete blade damage, is demonstrated.
- *Procedure 2* is a sensible approach used to identify and infer the degree of discrete blade damage based on a probabilistic blade damage threshold criterion.

5.1.1. Procedure 1

The results in this subsection do not demonstrate the proposed damage identification process, but rather demonstrates the ability of the proposed stochastic hybrid approach to track small changes in the natural frequencies of the test blades. The BTT results and FEM modal analysis results are therefore directly compared to one another in this subsection. As stated in Section 2, the relative change in the natural frequency of the test blade (blade 2) was tracked for changes in the size of the discrete blade damage (corresponding to the values in Table 1).

Figure 13 shows the change in the natural frequency at the various discrete crack sizes as determined from the amplitude and phase results. The 95% confidence intervals indicate that there is a reasonable amount of uncertainty for the BTT phase results of the healthy blade. In contrast, the greatest uncertainty of the BTT amplitude results occurs close to the greatest damage increment. The mean natural frequencies of the amplitude results decrease monotonically as the crack size increases. The mean of the amplitude results exhibit a decrease in the natural frequency of smaller than 0.2Hz between damage increments 2 and 3 for example, therefore demonstrating the ability of this stochastic approach to track small changes in the natural frequency while incorporating uncertainty. Both the amplitude and phase results, however, exhibit a number of humps in the mean natural frequencies. These humps may be indicative of areas of greater uncertainty. When comparing the results from the individual measurements it is unclear whether the *OROS* or *Genesis* DAQ performed better. There is a reasonable amount of scatter in both sets of results and outliers occurred for both DAQs.

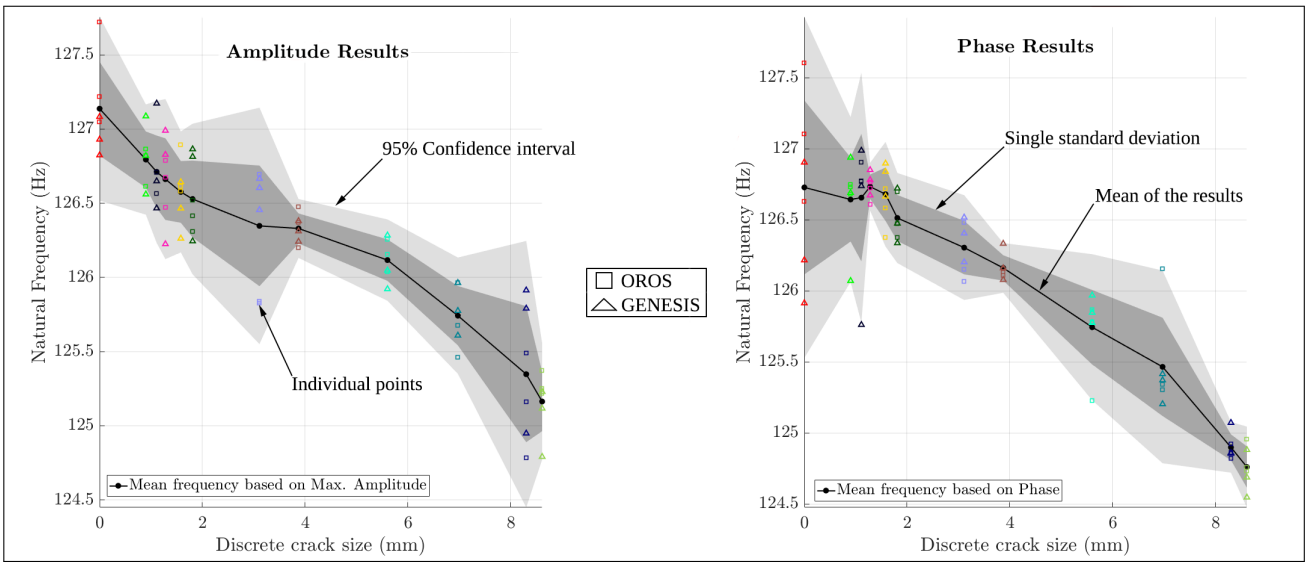

Figure 13: BTT natural frequency results for the amplitude and phase (blade 2).

Figure 14 compares the natural frequencies determined from the FEA and BTT methodologies. The relative error between the mean natural frequency results at the various damage increments are also compared. The following is deduced from Figure 14:

- The mean BTT amplitude and phase results indicate a maximum relative error of just under 0.4% for the natural frequency. In essence, the mean results are a very close match. The confidence intervals around the means of these result sets vary somewhat. This suggests that these result sets might work well in tandem; i.e. the phase results may give a more confident answer when there is greater uncertainty for the same set of amplitude results and vice versa.
- The FEM results, similar to the BTT phase results, indicate the greatest degree of uncertainty for the natural frequency of the undamaged blade. The confidence interval remains more or less uniform around the mean results thereafter.
- The relative error plots indicate that the FEM and BTT amplitude results are more consistently a closer match, with a maximum relative error of approximately 0.95%. The FEM natural frequencies also decrease monotonically, as would be expected for greater blade damage. The BTT phase results perform better for the largest damage increments when compared to the FEM results.
- The FEM results give a reasonably good projection of what may be expected in terms of the natural frequencies at the various damage increments.

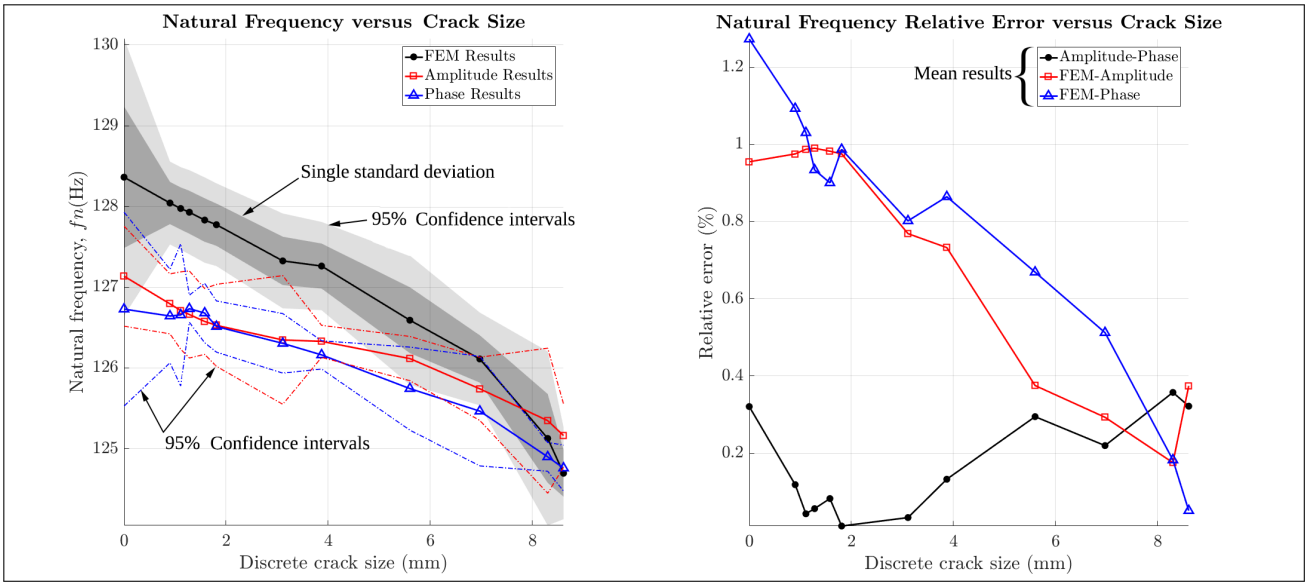

Figure 14: Comparison of the natural frequency at the damage increments (blade 2).

It is more sensible to track the change in the natural frequencies as a relative change, hence the term: *relative natural frequency tracking*. The implementation of the relative natural frequency tracking aims to give a more general indication of the blade condition, thus enabling a better basis of comparison between the various result-sets. The reference condition for this investigation is the natural frequency of the undamaged blade. Figure 15 shows the relative change in the natural frequency at the various discrete crack sizes. The relative discrete crack sizes are indicative of the fraction of the total width of the blade that is damaged. The calculation of the relative change in natural frequency (Δf_{n_i}) from the original natural frequency (f_{n_0}) to the current natural frequency (f_{n_i}) is shown in Equation 11:

$$\Delta f_{n_i} = \frac{f_{n_0} - f_{n_i}}{f_{n_0}} \times 100 \tag{11}$$

Figure 15 compares this relative change in the natural frequency of the test blade for the various approaches. The fitted curves through the mean data-points give an indication of relationship between the relative change in the natural frequency and the relative discrete crack size of the blade. However, these fitted curves do not intend to generalise this relationship. A number of different polynomials were tested to determine the best fit without resulting in over-fitting. Fitting a quadratic curve resulted in a lower Root-Mean-Square Error (RMSE) compared to a linear. Fitting a cubic polynomial resulted in over-fitting. Consequently, a quadratic polynomial was selected. Figure 15 shows that up to approximately 5% the relative FEM and BTT amplitude results are a close match. The fitted curve for the phase results follows a similar path to that of the FEM results, but exhibits a slight offset. Figure 15, however, shows that beyond 5% relative change in discrete crack size the mean BTT and FEM results start to diverge. Furthermore, at the largest damage increments for this investigation, the 95% confidence intervals of the BTT results no longer intersect the corresponding confidence intervals of the FEM results. This divergence needs to be accounted for in the damage identification process. This may possibly be achieved by being more conservative during the damage identification process; i.e. being more conservative when deciding whether a blade damage threshold has been reached. Another possibility is to perform model updating in the FEM modal analysis. However, this would require an inspection of the actual turbomachine blades to incorporate more complex aspects in the FEM modal analysis. More suggestions are presented in Section 5.1.2 alongside the demonstration of the damage identification process.

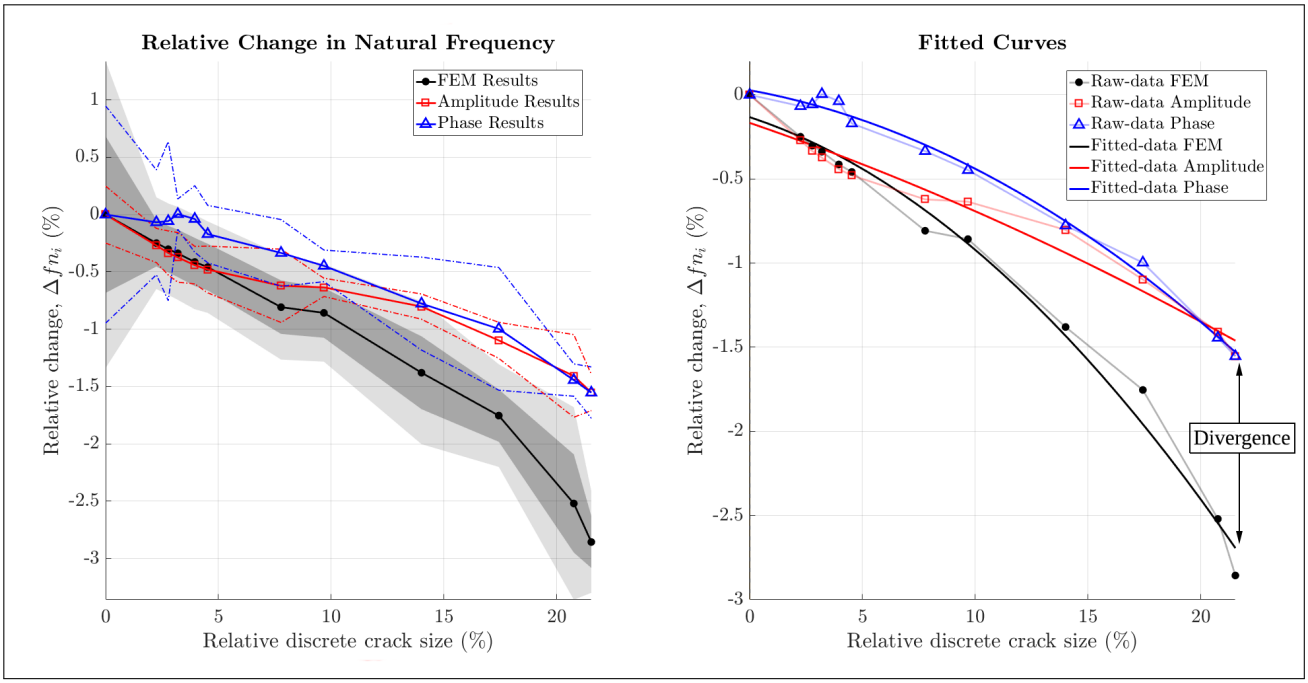

Figure 15: Comparison of the relative change in natural frequency at the damage increments (blade 2).

Section 3.4 discusses the possibility of combining the various BTT mean amplitude and phase signals at the respective frequencies. This differs to the preceding relative natural frequency tracking results in the sense that; once the complete range of amplitude and phase signals were combined or averaged, only then the associated natural frequencies are extracted. Figure 16 shows these combined mean amplitude and phase signals for the six corresponding tests at each damage increment. The features (represented by Equations 6 and 7) were extracted from the combined results and the associated natural frequencies, as shown in Figure 16, were found. The trace of the natural frequency indicates a decrease in the derived natural frequencies as the discrete damage increases. The derived natural frequency values using this approach tend to be slightly higher than the preceding approach where the natural frequencies were independently calculated.

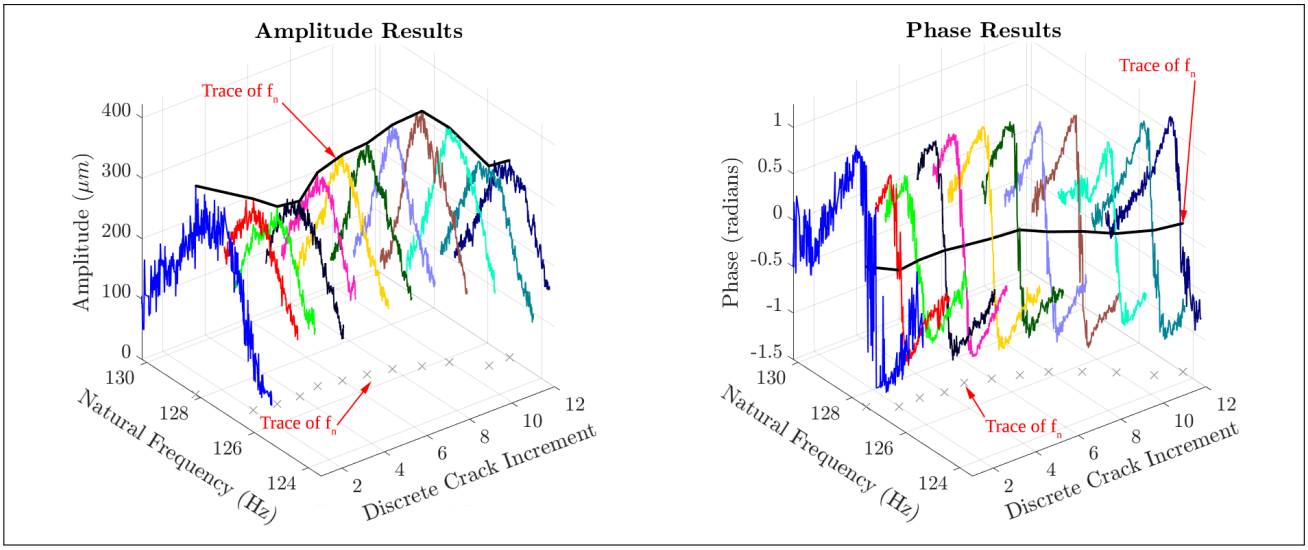

Figure 16: Demonstration of the archiving of the BTT signals for all the damage increments (blade 2).

This approach demonstrates the capabilities of using periodic BTT measurements to construct an *archive* of data over time. This would enable relative changes in the vibrational states of the blades to be tracked after similar signals are grouped together. For example, if a number of successive BTT measurements do not indicate a noticeable change in the derived natural frequencies, then these measurements may be grouped together and combined in this *archiving* scheme. The combined results shown in Figure 16 merely demonstrated the further potential of the BTT technique incorporating BLR. It is a major advantage of this BTT technique that the possibility exists to plot the entire range of amplitude and phase results over the local resonance domain; with the further possibility of establishing confidence intervals around the means of these results.

The results from both the relative natural tracking approaches indicate that very small changes in the natural frequency may be tracked. In some instances, relative changes of less than 0.2Hz were reported for the test blade due to small changes in the discrete damage size. The FEM modal analysis results provided a basis of comparison for the small relative changes in the natural frequency associated with a particular damage increment. This suggests that the proposed hybrid approach incorporating relative natural frequency tracking may be utilised for relatively small damage identification.

5.1.2. Procedure 2

This subsection demonstrates how the relative natural frequency tracking results may be used to identify and infer the degree of discrete blade damage based on a predetermined blade damage threshold criterion. Consequently, this section demonstrates the use of a blade damage identification procedure (based on a stochastic hybrid approach) used to determine whether a turbomachine outage should be scheduled.

It should be emphasised that *Procedure 2* assumes that the actual discrete damage sizes of the blades are not known. *Procedure 2* therefore relies on the tracking of the relative changes of the derived natural frequency BTT results to infer the degree of discrete blade damage. The FEM modal analysis facilitates the estimation of expected blade conditions (relative change in natural frequency) corresponding to a particular discrete damage size that is deemed critical. This set of FEM modal analysis results may then be used to establish a *damage threshold*. The aim of the damage identification procedure is to determine whether there is sufficient evidence from the stochastic hybrid approach to suggest that this damage threshold has been reached, thus resulting in a turbomachine outage.

Figure 17 shows two iterations of the proposed identification procedure. Only the BTT relative natural frequency tracking results are plotted (based on the amplitude and phase results). The BTT relative natural frequency results in Figure 17 correspond to the BTT results in Figure 15. Very important to note is that the BTT relative natural frequency results are no longer plotted against the relative discrete crack size in Figure 17. These results are now simply plotted according to the BTT test number; in industry this could be a date or time. Also note that the FEA relative natural frequency results are not used directly. Instead, a predetermined damage threshold is established using the FEM modal analysis results. The following steps describe the proposed damage identification procedure:

1. Define a level of discrete blade damage that would justify a turbomachine outage / inspection. In Figure 17 this is indicated by *Level 1*. This level corresponds to increment 5 of the FEA results or 1.58mm of discrete blade damage (3.95% relative discrete crack size). This level is arbitrarily chosen for the purposes of the damage identification demonstration. In practice, the principles of fracture mechanics and / or fatigue analysis can be used to define the *Level 1* blade damage threshold.

2. The FEM modal analysis was performed stochastically at this discrete crack size in order to quantify uncertainty. It is therefore essential to record the mean (μ_{FEM_1}) and standard deviation (σ_{FEM_1}) of the FEM results corresponding to this damage increment (*Level 1*).

3. A new variable, δ_{damage}, is defined as shown in Equation 12. This variable represents the difference between the relative change in the natural frequency of the BTT results (for a particular batch of tests) and the relative change in natural frequency of the FEM results at a particular discrete damage size (represented by *Level 1* in Figure 17).

$$\delta_{damage} = \Delta f_{n_{BTT}} - \Delta f_{n_{FEM}}(K) \tag{12}$$

In Equation 12, K denotes the predetermined crack size of the FEM modal analysis. It is very important to note that δ_{damage} is not a deterministic value, but rather a normal probability distribution. The reason being that both $\Delta f_{n_{BTT}}$ and $\Delta f_{n_{FEM}}(K)$ have associated normal distributions, summarised as follows:

$$\Delta f_{n_{BTT}} \sim \mathcal{N}\Big(\mu_{_{BTT}}, \sigma^2_{_{BTT}}\Big) \tag{13}$$

$$\Delta f_{n_{FEM}}(K) \sim \mathcal{N}\Big(\mu_{_{FEM}}, \sigma^2_{_{FEM}}\Big) \tag{14}$$

The associated normal probability distribution of δ_{damage} is the difference between the independent normal distributions of the BTT results (Equation 13) and FEM results (Equation 14). The formulation of the normal probability distribution of δ_{damage} is shown in Equation 15:

$$\delta_{damage} \sim \mathcal{N}\Big(\mu_{_{BTT}} - \mu_{_{FEM}}, \sigma^2_{_{BTT}} + \sigma^2_{_{FEM}}\Big) \tag{15}$$

4. The calculation of the mean and variance of δ_{damage} (as shown in Equation 15) requires that a number of repetitive BTT tests are performed. Repetitive tests essentially enable the mean, $\mu_{_{BTT}}$, and standard deviation, $\sigma_{_{BTT}}$, of a certain batch of BTT tests to be determined.

5. The probability, $P(\delta_{damage} \leq 0)$, is determined for a particular batch of BTT tests and chosen $\Delta f_{n_{FEM}}$ (*Level 1* in this case). This probability is found from the Cumulative Distribution Function (CDF) of δ_{damage}, with associated mean and variance as shown in Equation 15. $P(\delta_{damage} \leq 0)$ is the probability that the relative change in the natural frequency derived from the BTT measurements ($\Delta f_{n_{BTT}}$) equals or exceeds the permissible relative change in the natural frequency derived from the FEM analysis ($\Delta f_{n_{FEM}}(K)$).

6. The damage threshold (X_{dt}) is based on a selected probability, $P(\delta_{damage} \leq 0) > X_{dt}$. It is up to the user to decide what an *acceptable* probability is to justify a turbomachine outage. Repetitive BTT tests are conducted in intervals until this probability value (damage threshold) is reached. Once this damage threshold is reached a turbomachine outage will be scheduled and the necessary inspections of the damaged blade will commence. If necessary, this blade may be replaced if the damage on the blade is deemed critical. It is important to note that the damage threshold (X_{dt}) may be selected as a conservative value. The choice of the value of the damage threshold may differ depending on the particular application of this procedure; it is entirely up to the user to decide what this value should be.

7. Steps 1 - 6 is repeated after every inspection or maintenance operation, until a blade needs to be replaced. After each inspection a new *damage level*, based on the FEM results will be prescribed to determine a new blade damage threshold.

Figure 17 demonstrates two iterations of the damage identification process. In this figure, *Level 1* corresponds to a relative discrete crack size of 3.95% (1.58mm) and *Level 2* corresponds to a relative discrete crack size of 9.675% (3.87mm). These levels were arbitrarily chosen and are merely used to demonstrate the damage identification process.

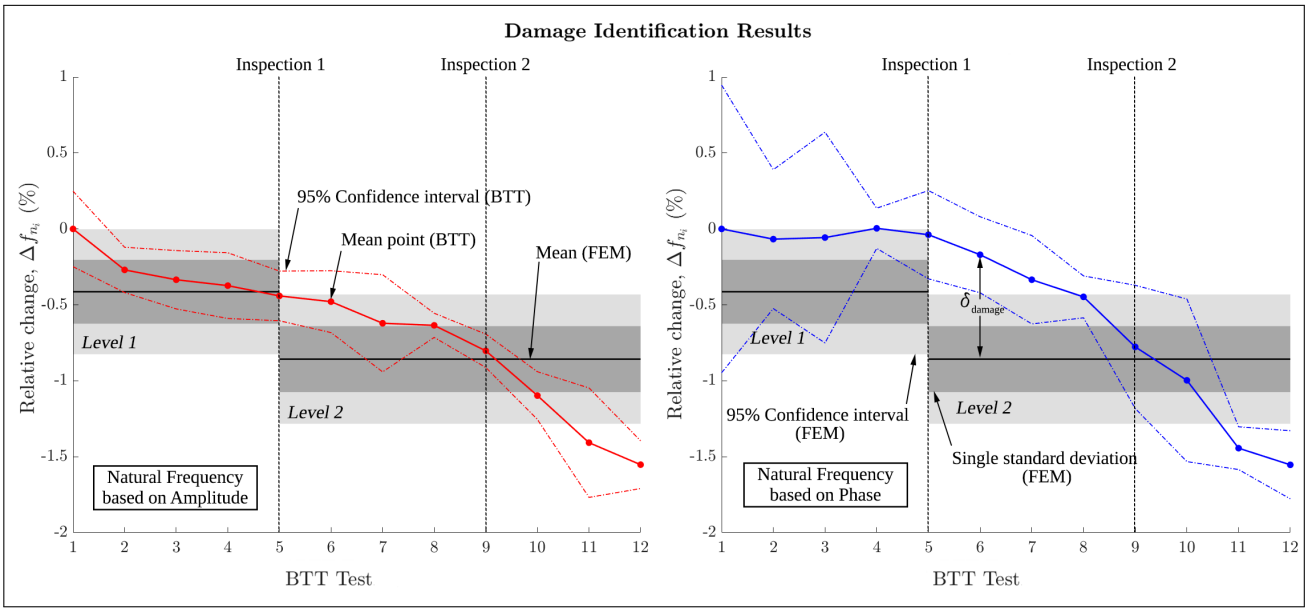

Figure 17: Damage identification results (blade 2).

Table 4 shows the derived probability, $P(\delta_{damage} \leq 0)$, for each batch of the BTT tests. In Table 4, P_{Amp} and P_{Phase} refers to the probabilities based on the BTT amplitude and phase results respectively. The following points summarise the outputs of the damage identification process for *Group II*:

- The first damage threshold is defined as $X_{dt_1} = P(\delta_{damage_1} \leq 0) > 0.5$ and relates to *Level 1*. This damage threshold implies that a turbomachine outage will be scheduled if there is a probability greater than 50% that $\Delta f_{n_{BTT}}$ exceeds $\Delta f_{n_{FEM}}(K_{Level_1})$. Based on the results in Figure 17 and Table 4, inspection 1 is performed after batch 5 of the BTT testing. According to Figure 15, the actual discrete blade damage is also 1.58mm (3.95% relative discrete crack size).

- After the first inspection a new reference position is established. The second damage threshold is defined as $X_{dt_2} = P(\delta_{damage_2} \leq 0) > 0.4$ and relates to *Level 2*. This damage threshold is chosen to be more conservative due to inspection 1 indicating that the blade is already damaged (close to 4%) and the fact that *Level 2* corresponds to approximately 10% discrete blade damage. It is advised to be more conservative with increasing blade damage. Based on the results in Figure 17 and Table 4, inspection 2 is performed after batch 9 of the BTT testing. According to Figures 14 and 15, the actual discrete blade damage is 5.6mm (14% relative discrete crack size) at this batch of BTT results. *Level 2*, however, represents 3.87mm of discrete blade damage in the FEA. Inspection 2 therefore proves that the FEM modal analysis and BTT relative natural frequency tracking results diverged for this discrete damage size. In practice, model updating would need to be performed in the FEA to correct this divergence.

- Table 4 shows that the probabilities, $P(\delta_{damage_2} \leq 0)$, for batch 10 - 12 are greater than 0.5. These values were merely computed for interest-sake. These probabilities imply that the mean of the relative natural frequencies of the BTT results have crossed-over the mean of *Level 2*. Figure 17 shows that this is indeed the case. For batch 12 the probabilities are very close to 1, due to fact that the 95% confidence intervals of the BTT results and *Level 2* no longer cross-over.

Table 4: Probabilities, $P(\delta_{damage} \leq 0)$, for the BTT relative natural frequencies based on the amplitude and phase results (blade 2).

BTT Test	$\boldsymbol{P_{Amp_1}}$	$\boldsymbol{P_{Phase_1}}$	$\boldsymbol{P_{Amp_2}}$	$\boldsymbol{P_{Phase_2}}$	
1	0.0458	0.2162			
2	0.2597	0.1350			
3	0.3665	0.1930			
4	0.4326	0.0292			
5	**0.5485**	**0.0719**	**Inspection 1**		
6			0.0579	0.0032	
7			0.1922	0.0234	
8			0.1569	0.0362	
9			**0.4035**	**0.3939**	**Inspection 2**
10			0.8501	0.6555	
11			0.9734	0.9948	
12			0.9987	0.9977	

5.2. Damage classification

The damage identification approach presented in Section 5.1 relies on repetitive or frequent measurements to be available. The damage classification approach, however, aims to facilitate the use of a single set of BTT measurements to determine the blade condition. For this scenario the mean of repetitive BTT measurements (corresponding to a particular discrete damage interval) would not be established, therefore requiring much confidence to be placed on a single measurement. The proposed damaged classification approach is based on the clustering of the BTT natural frequency and amplitude values. The clustering of these derived vibrational characteristics enable the severity of the blade damage to be classified. Many clustering techniques exist, with each technique ranging in complexity and functionality [1]. The proposed clustering technique for the hybrid approach shown in Figure 1 is *K-means clustering*. K-means clustering is a mature and popular technique whereby observations with the nearest mean are assigned to a certain cluster of data-points [17]. This physically translates into vibrational characteristics of a blade, from a specific BTT measurement, being assigned to an existing cluster of vibrational characteristics with the nearest mean. The aim of this K-means clustering approach is to classify the severity of the blade damage according to which group the vibrational characteristics of a particular BTT measurement are assigned to. Consequently, the severity of the blade damage may be determined from these clusters. The following points summarise this process:

- The vibrational characteristics (amplitude and associated natural frequencies) of a certain blade are extracted from the BTT measurements and used further in the clustering process.
- The clustering of the natural frequency and amplitude results using predetermined mean values is proposed. The predetermined mean values correspond to the natural frequency results from the FEM modal analysis, particularly for the first bending mode. Importantly, the amplitudes of vibration were not computed during the FEM modal analysis. A Computational Fluid Dynamics analysis would be required to simulate the fluid-flow interaction on the the blades used during experimentation. From this CFD analysis an indication of the amplitudes of blade vibration could be determined. This CFD analysis was not performed for the following reasons:
  - The proposed hybrid approach aims to meet the requirement of a simple implementation.
  - Further investigations of the *K-means clustering* implementation used in this research showed that it would be sensible to assign *zero* amplitude values to these initial clusters.

- It was decided to partition the data into three initial clusters (*k mean clusters*, hence the name *K-means clustering*). These initial clusters correspond to the assigned zero amplitude values and predetermined mean natural frequencies from the FEA. The partitioning of the data corresponds to the discrete damage increments shown in Table 1. Each partition was classified according to severity of the blade damage it represented, thus indicating the non-severe damage increments, mid-severity damage increments and most severe damage increments respectively (also indicated in Table 1). It is important to note that these partitions were not enforced on the BTT data before the K-means clustering commenced. However, after the clustering was completed the individual natural frequency points (shown in Figure 13) and associated amplitudes were used to determine the accuracy of the final classification into the various ranges of damage.
- The initial cluster centres correspond to the zero amplitude values and the mean natural frequency values of the FEA results partitioned using the aforementioned scheme. This resulted in three amplitude and natural frequency combinations / locations used as a starting point of the centroids. These initial cluster centres thus enabled individual BTT measurements to be classified to the closest partition.
- It is important to scale the BTT amplitude and natural frequency data for the use in the K-means clustering; i.e. normalise the data so that the values of both the amplitudes and natural frequencies ranged between 0 and 1. This normalisation was done according to the minimum (assigned to 0) and maximum (assigned to 1) of these data-points. The initial cluster centroids (FEM natural frequency data) was also scaled using this scheme. The amplitudes of the initial cluster centroids were already zero and therefore did not require scaling. This was an important step before the K-means clustering commenced as it ensured that neither of these values (amplitude or natural frequency) dominated the Euclidean distance formulation.
- The point-to-cluster-centroid distances are computed for all of the individual BTT points. The BTT points are essentially treated as a *black-box*, with no indication of which damage increment the points belong to. The overall averages of the points in the clusters are calculated and new centroid locations are allocated. As a result the BTT points are classified into the associated group of most likely Range of Damage (RoD) that the amplitude and natural frequency would be representative of. In Figure 18 *RoD I*, *RoD II* and *RoD III* represent the new averaged clusters for the undamaged, middle damage and greatest damage increments respectively. The incorrectly classified BTT points along with the corrected classification group are also shown in Figure 18.

The results of the K-means clustering implementation as part of the damage identification process are shown in Figure 18. In Figure 18 *RoD I*, *RoD II* and *RoD III* represent the new averaged clusters for the non-severe, mid-severity and severe damage increments respectively. The incorrectly classified BTT points are also shown in Figure 18; the correct classification for these incorrectly classified points are indicated by a Roman Numeral above the marker. These corrections were possible due to the fact that the actual BTT measurements were available before the classification commenced. In practise, these corrections may rely on the results from the *damage identification* procedure, where a certain discrete crack size is inferred. The following points should be noted regarding the accuracy of the K-means clustering implementation:

- The the overall classification accuracy is 78% (56 out of the 72 points were correctly classified) according to the imposed partitions of the damage increments shown in Table 1.
- If only the *RoD III* (severe classification) is considered as important for determining whether a damage threshold has been reached, then this classification accuracy would be 94% accurate (4 out of the 72 points were incorrectly classified for this particular partition). This specific partition would put a greater emphasis on *RoD III*, therefore grouping *RoD I* and *RoD II* together.

It is, however, a great concern when an actual *RoD III* (severe) point is classified as a *RoD I* (non-severe) point. This, however, only occurred for a single data-point.

- When considering the damage increments or RoDs independently, the following is reported for the resultant K-means clustering accuracy for this implementation:
  - *RoD I*: Only 26 out of the 36 possible points are correctly classified, therefore resulting in a 72% accuracy when this RoD is considered independently.
  - *RoD II* and *RoD III*: For both these RoDs, only 15 out of the 18 possible points are correctly classified, therefore resulting in a 83% accuracy when these RoD are considered independently.

It should be reiterated that an incorrect classification of an actual *RoD III* point would be regarded as critical, especially when a data-point from this RoD is assigned to *RoD I*. It is hypothesised that the accuracy of the classifications may improve if additional features, resulting in more definitive cluster locations, are implemented. It is recommended for future iterations of the proposed clustering approach to consider additional features. The consideration of additional features may be possible when a more complex CFD fluid-flow interaction analysis for a particular blade is implemented. The phase information could possibly be incorporated along with the natural frequencies associated with this phase information. Additional features do not necessarily imply greater accuracy. If these additional features do not result in more definitive cluster locations, the accuracy of the final prediction may decrease drastically.

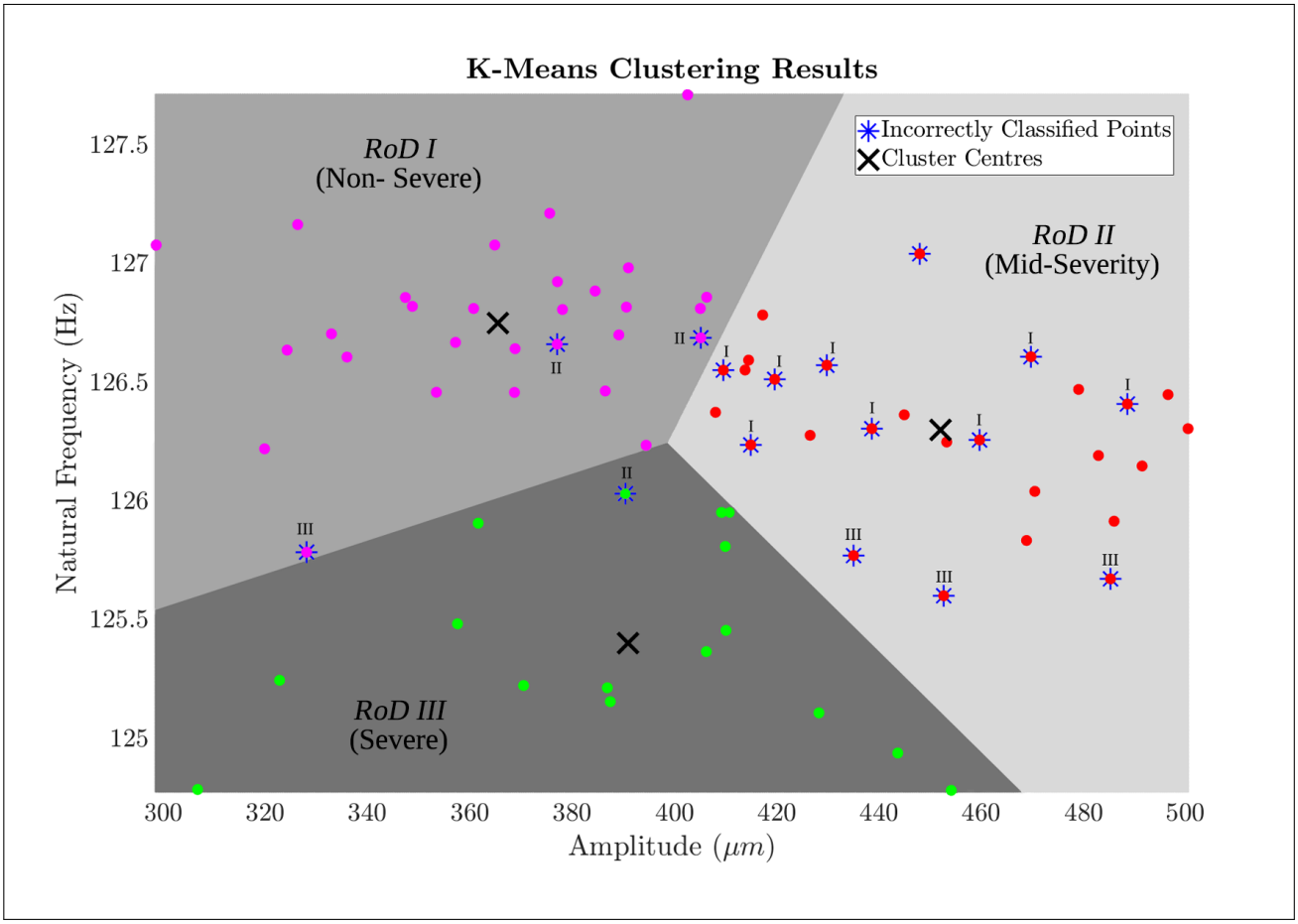

Figure 18: Illustration of the K-means clustering results.

For practical applications, it is proposed that the K-means clustering implementation should supplement the hybrid approach outlined in Figure 1. The clustering of the BTT results to predetermined centres would allow the blade damage to be classified according to k-partitions imposed on the data. The damage threshold may be chosen based on these damage classifications. The following outcomes are possible for this proposed blade damage classification strategy:

1. The derived amplitude and natural frequency results are classified as *non-severe* (*RoD I*). This could potentially signify that the blade is still in good condition. As indicated in Figure 18, numerous points were incorrectly classified as *RoD I*. This may be a concern, especially if a *RoD III* point is incorrectly assigned to *RoD I*.
2. If these values are classified as *mid-severity* damage (*RoD II*) then this would give an indication that the condition of the blade is potentially deteriorating.
3. Lastly, if these values are classified as *severe* damage (*RoD III*) then this would indicate that the blade damage is immense, therefore signifying a damage threshold being reached and resulting in a turbomachine outage being scheduled.

6. Conclusion

Industry is increasingly confronted by ageing turbomachines prone to unexpected and catastrophic failure. This raises questions with regards to the safety and optimal outage planning of these turbomachines. The consulted literature highlighted that BTT is a promising technique to monitor and provide an early warning of critical turbomachine blade conditions. BTT offers the ability to monitor all the blades in a stage of a turbomachine while also being a non-intrusive and non-contact approach. There is no consensus in published literature as to which BTT algorithm attains the highest accuracy, partly due to the difficulty associated with validating these results. The purpose of this paper is therefore to advance the state of the art in BTT technology into a stochastic hybrid approach, used for the identification and classification of turbomachine blade damage. This stands in stark contrast to the vast majority of current BTT research where purely data-driven approaches are used, most of them being deterministic in nature. This hybrid approach uses the outputs of a recently developed BTT technique based on BLR and a stochastic FEM modal analysis. The hybrid implementation aims to provide a simple solution to alleviate the disadvantages of the individual analysis types while conserving the advantages.

An experimental rotor setup was used during the BTT investigations, therefore providing experimental data for the use in the proposed hybrid approach. In doing so, discrete damage was incrementally introduced to a test blade, thus facilitating the testing of the damage identification and classification approaches. The damage identification procedure is based on the probability that the relative change in the natural frequency of the BTT results is as large as what the FEM modal analysis (at a chosen discrete damage size) projected it to be. This probabilistic damage identification procedure demonstrated the ability of to infer the degree of blade damage. The damage classification approach facilitates the use of a single set of BTT measurements to determine the blade condition. In an attempt to meet the requirement of a simple implementation, K-means clustering is used to classify the derived BTT amplitude and natural frequency values. The predetermined FEM natural frequency results are used to initiate clusters and cluster centroids. The clustering of the derived BTT vibrational characteristics to the nearest cluster centroid enable the severity of the blade damage to be classified. The damage classification results, however, showed that there is the possibility of incorrectly classifying a severely damaged blade as non-severely damaged. This scenario could potentially have serious implications in practice. Future research should therefore investigate the performance of a number of different classification algorithms.

Furthermore, the proposed hybrid approach should ideally be tested on an actual turbomacine exposed to practical working conditions. This would provide a more convincing conclusion regarding the applicability of the proposed hybrid approach for the use in industry. Overall, it may be concluded that the use of a stochastic hybrid approach for blade condition monitoring has many advantages. The main advantage is that uncertainty is considered throughout the approach. For example, this enabled a probabilistic indication of the blade condition to be established for the damage identification. Furthermore, the fusion of the results from the various analyses consistently provided a more confident indication of the condition of the test blade, resulting in supporting evidence of whether a practical maintenance decision should be made.

Acknowledgements

The use of the Genesis High Speed DAQ was graciously made possibly by *ESTEQ Gauteng*. The authors also acknowledge the support of the Eskom Power Plant Engineering Institute (EPPEI) in the execution of this work.

References

[1] M. Mishra, J. Saari, D. Galar, and U. Leturiondo. Hybrid models for rotating machinery diagnosis and prognosis estimation of remaining useful life. Technical report, Luleå University of Technology, May 2014.

[2] L. Liao and F. Köttig. Review of hybrid prognostics approaches for remaining useful life prediction of engineered systems, and an application to battery life prediction. *IEEE Transactions on Reliability*, 63(1):191–207, 2014.

[3] J.Z. Sikorska, M. Hodkiewicz, and L. Ma. Prognostic modelling options for remaining useful life estimation by industry. *Mechanical Systems and Signal Processing*, 25(5):1803–1836, 2011.

[4] R.P. Dewey, N.F. Rieger, and T. McCloskey. Survey of steam turbine blade failures. *EPRI CS-3891 project*, 1, 1985.

[5] G. Rigosi, G. Battiato, and T.M. Berruti. Synchronous vibration parameters identification by tip timing measurements. *Mechanics Research Communications*, 79:7–14, 2017.

[6] B. Salhi, J. Lardies, and M. Berthillier. Identification of modal parameters and aeroelastic coefficients in bladed disk assemblies. *Mechanical Systems and Signal Processing*, 23(6):1894–1908, 2009.

[7] R. Rzadkowski, E. Rokicki, L. Piechowski, and R. Szczepanik. Analysis of middle bearing failure in rotor jet engine using tip-timing and tip-clearance techniques. *Mechanical Systems and Signal Processing*, 76:213–227, 2016.

[8] A.R. Rao and B.K. Dutta. In situ detection of turbine blade vibration and prevention. *Journal of failure analysis and prevention*, 12(5):567–574, 2012.

[9] D.H. Diamond, P.S. Heyns, and A.J. Oberholster. A comparison between three blade tip timing algorithms for estimating synchronous turbomachine blade vibration. In *9th WCEAM Research Papers*, pages 215–225. Springer, 2015.

[10] J.S. Rao. *Turbomachine blade vibration*. New Age International, Delhi, 1st edition, 2010.

[11] R.G. Budynas and J.K. Nisbett. *Shigley's Mechanical Engineering Design*. McGraw-Hill, New York, 9th edition, 2011.

[12] J. Gallego-Garrido, G. Dimitriadis, I.B. Carrington, and J.R. Wright. A class of methods for the analysis of blade tip timing data from bladed assemblies undergoing simultaneous resonances—Part II: Experimental validation. *International Journal of Rotating Machinery*, 2007, 2007.

[13] M.Á. Herrador and A.G. González. Evaluation of measurement uncertainty in analytical assays by means of Monte-Carlo simulation. *Talanta*, 64(2):415–422, 2004.

[14] S. Madhavan, R. Jain, C. Sujatha, and A.S. Sekhar. Vibration based damage detection of rotor blades in a gas turbine engine. *Engineering Failure Analysis*, 46:26–39, 2014.

[15] Field demonstration of low-pressure turbine blade stress monitoring. Technical Report 1024665, EPRI, Palo Alto, CA, 2012.

[16] C. Booysen, P.S. Heyns, M.P. Hindley, and R. Scheepers. Fatigue life assessment of a low pressure steam turbine blade during transient resonant conditions using a probabilistic approach. *International Journal of Fatigue*, 73:17–26, 2015.

[17] K. Wagstaff, C. Cardie, S. Rogers, S. Schrödl, et al. Constrained k-means clustering with background knowledge. In *ICML*, volume 1, pages 577–584, 2001.